Spring 5-11-2019

Paper Structure Formation Simulation

Tyler R. Seekins
University of Maine, tyler.seekins@maine.edu

Follow this and additional works at: https://digitalcommons.library.umaine.edu/etd

Part of the Dynamic Systems Commons, Numerical Analysis and Computation Commons, Probability Commons, Statistical Models Commons, and the Wood Science and Pulp, Paper Technology Commons

PAPER STRUCTURE FORMATION SIMULATION

By

Tyler R. Seekins

B.S. Chemical Engineering, University of Maine, 2011

A THESIS

Submitted in Partial Fulfillment of the

Requirements for the Degree of

Master of Science

(in Chemical Engineering)

The Graduate School

The University of Maine

May 2019

Advisory Committee:

Douglas W. Bousfield, Calder Professor of Chemical and Biomedical Engineering, Advisor

Andre Khalil, Associate Professor of Chemical and Biomedical Engineering

Peter Stechlinski, Assistant Professor of Mathematics

PAPER STRUCTURE FORMATION SIMULATION

By Tyler R. Seekins

Thesis Advisor: Dr. Douglas W. Bousfield

An Abstract of the Thesis Presented
in Partial Fulfillment of the Requirements for the
Degree of Master of Science
(in Chemical Engineering)
May 2019

On the surface, paper appears simple, but closer inspection yields a rich collection of chaotic dynamics and random variables. Predictive simulation of paper product properties is desirable for screening candidate experiments and optimizing recipes but existing models are inadequate for practical use. We present a novel structure simulation and generation system designed to narrow the gap between mathematical model and practical prediction. Realistic inputs to the system are preserved as randomly distributed variables. Rapid fiber placement (1 second/fiber) is achieved with probabilistic approximation of chaotic fluid dynamics and minimization of potential energy to determine flexible fiber conformations. Resulting digital packed structures, storable in common formats, return basic properties and provide a flexible platform for subsequent analysis and prediction. Simulated results are validated through comparison with experimental handsheet measurements. Good agreement with thickness measurements are obtained and possible uses of simulated structures for more enhanced property prediction are discussed.

DEDICATION

To Stephanie, for your encouragement while I pushed my limits, and your patience and
loyalty through frustration and failure.

ACKNOWLEDGEMENTS

TABLE OF CONTENTS

LIST OF TABLES

LIST OF FIGURES

CHAPTER 1
INTRODUCTION

In the mature industries like papermaking, incremental improvements lead to large advantages. Manufacturers compete to improve or maintain product performance and profit margins. A growing selection of fibers, additives, and coatings leads to unlimited potential recipes. Access to greater volumes of higher resolution information is a competitive advantage.

Experimentation in a lab can be costly, time consuming, and messy. Furthermore many experiments or measurements often require consistent human attention. This problem only compounds with scale. While manufacturing facilities are at least mostly automated, in depth experimentation with process conditions is rare. With these constraints it's not usually feasible to fully explore the space of all input combinations. This makes optimization by direct observation of process and property variables difficult.

One mitigating approach to this challenge is to develop simulations capable of predicting the relevant variables and optimize them directly. Where considerable time and individual attention is required to collect large sets of lab data, simulation allows for automatic generation of data limited only by the duration of the simulation and the computational resources available. Simulations also allow for exploration of a wider range of conditions than is feasible at manufacturing scale.

Technology provides a growing ensemble of instrumentation and techniques to probe and predict the natural world. However, the internal mechanisms of many natural processes are still not possible or practical to directly observe. Modeling and simulation emerge as cost effective tools to unravel otherwise invisible connections. From observation, first principles, and intuition, we can synthesize rules that extend to the unobservable. We consider our models useful abstractions of real systems if they allow us to predict outcomes in new situations, optimize inputs, or improve understanding.

While accurate process scale simulation of gas and liquid chemical systems has been effective for decades [1] [2], simulations involving solids remain problematic. In addition to heterogeneity of possible structures and conformations, solid materials interact with each other in complex and intractable ways. The formation of paper, for example, is a complex, chaotic process in which a collection of randomly shaped and oriented fibers are separated by filtration from a liquid slurry. Fully simulating every fluid and particle dynamic during the formation is almost inconceivably complex, however it happens in the real world in a matter of seconds. Even if this system could be simulated for a meaningful area in a human time scale it's highly chaotic and would exhibit a large degree of sensitive dependence to inputs that are already randomly distributed by natural processes.

We describe a versatile framework to simulate the placement of particles and flexible fibers. Random samples of fibers are generated from measured particle size distributions. Chaotic fluid dynamics controlling particle placement are approximated using a flux based probability measure. The final conformation of the flexible fibers is determined by optimizing a balance between the fiber curvature and distance from the forming surface. We conclude by discussing strategies to connect simulation and physical property predictions.

CHAPTER 2
BACKGROUND

Without providing a comprehensive review of particle packing literature, we highlight simulation types across the spectrum of realism, introduce the concept of chaos and probabalistic representations thereof, and provide a description of the open source platforms used in the development of this work. A summary of simulation types is given in Table 2.1.

2.1 Dynamic Packing Simulation

One possible approach to the study of paper structure formation is to collect detailed mathematical descriptions of all relevant forces acting on all particles in the system and solve the resulting equations of motion of the system through time.

2.1.1 Stokesian Dynamics

Stokesian Dynamics is an established technique to simulate the motion of multiparticle systems subject to deterministic and stochastic forces. Particles are treated as rigid spheres subject to hydrodynamic, interparticle, single particle, and brownian motion forces. Due to the realistic treatment of forces, different chemical, hydrodynamic, and even magnetic effects can be studied in detail. Sand et al. [3] share a model using this technique to describe the mobility and consolidation of small particles during the drying of a paper coating and study the influence of various interactions on the drainage rate and packing density. Although extremely detailed, the computation is costly, even for small systems. Furthermore, reported results are limited to uniform or mixed size spherical particles and use of the technique to place non-spherical particles is not clear at present. As a result the method is not suitable for the study of paper sheet formation.

2.1.2 Flexible Fiber Consolidation

Lavrykov et al. [4] describe a detailed model for the rigorous simulation of sheet formation and wet pressing. In the formation stage, fluid flow around the fibers is governed by the Navier-Stokes equations. Fibers are represented in this stage as chains of rigid, cylindrical segments, subject to deterministic forces from the fluid and each other. Different sections of the forming machine are incorporated through the use of time varying boundary conditions. Following formation, the jointed beams are replaced by realistic fiber geometries defined by a finite element mesh and the deformation of the fiber network subject to mechanical forces is simulated. While the simulation is detailed and allows the direct prediction of tensile strength using the same FEM analysis as the wet pressing, computation time is costly. The author reports that the generation of a representative sheet is completed in approximately six hours.

2.2 Chaos

As a motivation for the next class of models described, it is helpful to develop an intuition for the mathematical connection between deterministic dynamical systems and stochastic systems. The quickest path is to demonstrate the large effect small changes in initial conditions can have on the trajectories of even simple dynamical systems. The most famous example is the deceptively simple, recursive, discrete, dynamical system known as the logistic map.

$$x_{k+1} = 4 \ x_k \ (1 - x_k) \tag{2.1}$$

Given an initial condition, X_0, an infinite sequence of points can be produced by substituting the outcome on the left side of the equation into the map on the right. Although equilibrium points and multi-period orbits exist, such rational numbers are not possible to express in a floating point decimal system. As a result, even when such initial conditions are specified, tiny errors propagate into an easily observable manifestation of

(a) Logistic Map Orbits x_k Vs k   (b) Histogram of Iterates and the Beta Distribution
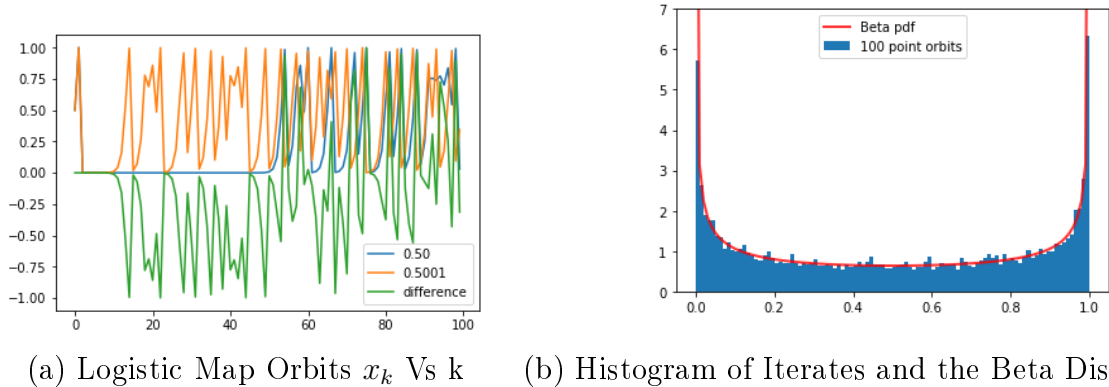
Figure 2.1. The Logistic Map and Beta Distribution

chaos. This outcome is shown in Figure 2.1 for initial conditions of 0.50, analytically a fixed point in blue, and 0.5001 in orange. The difference between the two orbits is plotted in green. Despite the inherent unpredictability of individual orbits beyond the horizon of chaos, chaotic attractors are bounded. In fact, any attractor can be represented using a probability measure in that each point has a well defined probability of mapping arbitrarily close to any other point in the interval. For this example, orbits of the logistic map are shown to be beta distributed with parameters $a = b = 0.5$ [5].

While chaos is not present in every dynamical system, and although we present no formal proof, it's presence in the formation of packed structures is easily apparent. Chaotic fluid dynamics means exact replication of structures in the lab is impossible. However, generation of exact structures is unnecessary if instead the distribution of possible outcomes can be obtained. While the advantage of simulations described above lies in their detailed representation of fluid and particle interactions, their computational complexity prohibits their use in the exploration of a large experimental space. Additionally, sensitive dependence on initial conditions and random inputs means a representative distribution of outcomes is unlikely to be obtained in this way, motivating a more probabilistic approach.

2.3 Random Packing

Simulations described in previous sections form packings through determination of the trajectories of all particles in the system throughout formation. Motivated by a simple example of chaos, we can instead consider the final resting place of each particle as a random sample from the set of possible locations over the structure. The most naive of such approximations assuming each particle has an equal chance of landing at any point in the horizontal xy plane.

2.3.1 Voxel Methods

Byholm et al. [6] describe a volumetric pixel, voxel, based technique to generate packings of particles with complex geometries. Their simulation is in a sense dynamic in that it evolves through time in fixed length steps. Unlike previous simulations, particle motion is entirely random. Particles are periodically introduced at the rising top boundary of the simulation and allowed to translate and rotate a small random amount, subject to collision detection, each time step. Particles who have not moved for some period are frozen and no longer simulated to mitigate memory consumption. The computational cost, both in time and memory, of voxel methods scales with the resolution of the 3-d simulation grid. The authors report packing times of two hours for a grid size of 800^3 although this varies based on the number of particles to be simulated and their complexity. This class of simulation, although most robust for complex particle geometries, is not suited to non-rigid particles, and thus insufficient for the simulation of paper fibers.

2.3.2 Analytical Models of Random Fiber Networks

An excellent review of analytical packing models, approached through statistical geometry is given in [7]. Several results are shared for 3-d random networks, however the theory for 2-d networks is substantially more developed. Many exact results for pore size,

density, and fiber to fiber contacts are shared in terms of named probability distributions for planar networks.

2.3.3   KCL-PAKKA

The KCL-PAKKA model, first described in 1994 [8] and in greater detail in 1997 [9] and 1998 [10], has earned a reputation in literature for its efficient generation of representative paper structures. While dynamic, mechanistic simulations previously described take hours, a PAKKA simulation was designed to take minutes, in the 1990's.

The PAKKA simulation's efficiency stems from its simplified forming rules and representation of the fiber and sheet structure. The height profile of the sheet is represented as a topographical surface and discretized into a grid. Instead of simulating the entire network during formation, fibers, also discretized, are placed one at a time, with uniform probability over the entire grid and with uniform, or otherwise distributed, probability of in plane rotation. Given a fibers location, a slice from the topography is extracted and the sheet height is updated at each element in the slice. The final height of the elements of each fiber are determined by restricting the maximum difference between adjacent elements and then allowing the height of each element of the fiber to decrease until it reaches the height of the existing topography or reaches the maximum displacement. Fines and fillers are incorporated by placing single elements on the grid such that their mass fractions are consistent with real pulp. Once placed, fibers are fixed, and dynamics beneath the surface of the forming structure are not considered.

Conceição et al. [11] present a cellular automata formulation of the PAKKA model implemented in MatLab. A smoothing mechanism is included to simulate drainage. The mechanism functions by rejecting, with a user defined probability, the location of a fiber if its final height is greater than its neighbors.

There are numerous references to the usage of PAKKA structures for further simulation as well. Bakhta et al. [12] study the seepage of ink into PAKKA structures using the

Table 2.1. Summary of Simulation Types

	Placement Strategy	Realism	Fibers
Stokesian Dynamics	Dynamical Simulation	High	No
Finite Element Consolidation	Dynamical Simulation	High	Yes
Analytical Methods	Random	Low	Yes
Voxel Methods	Random	High	No
KCL-PAKKA	Random	Moderate	Yes

	Complex Shapes	Computation Speed
Stokesian Dynamics	No	Slow
Finite Element Consolidation	Yes	Slow
Analytical Methods	No	Fast for 2-d
Voxel Methods	Yes	Moderate
KCL-PAKKA	No	Fast

Lattice Boltzmann method. Aurela et al. [13] simulate transport of volatile compounds through paper using representative structures generated by the PAKKA model.

While effective, the PAKKA model has several significant drawbacks. First, no attempt is made to incorporate the effect of drainage on the structure. Second, limiting the displacement of adjacent fiber elements means the slope is limited and curvature is not considered at all. If the fibers are supposed to be perfectly stiff, then the displacement is limited to zero which means the fibers would be perfectly flat. In real systems, these fibers, although inflexible would tip. This highlights an additional non-ideality. The assumed length of the fibers placed is that of the horizontal fiber. When adjacent elements are allowed to be displaced, even by a limited amount, the length of the placed fiber will be longer than assumed.

The simulation described in the following chapters of this thesis most closely resembles the PAKKA model. We maintain the process of evolving a 2-d topography to generate detailed 3-d structures but the similarities end there. We derive a novel probability measure to represent chaotic fluid dynamics and develop new bending rules that more realistically represent the curvature of the fibers, displays more realistic behavior as stiffness increases infinitely, and mitigates the elongation problem.

2.4 Python and Open Source Scientific Computing Framework

The implementation platforms of previously described simulations span a wide spectrum from FORTRAN to Commercial Finite Element Modeling Software. Integral to the implementation of the new work described in the following sections is the scientific computing stack. Requirements considered when choosing the simulation environment fall under three categories, computation speed, implementation speed, open source access. This requires the platform is stable, has an established, comprehensive support structure and community for trouble shooting, and implements most necessary functionality.

The system described in this thesis was built from the ground up using only two open source python packages, NumPy [14] and SciPy [15] [16] plus the Python language for core computation, one open source Python package for two dimensional visualization and analysis, MatPlotLib [17], and another open source software package, ParaView [18] for rendering in detail the three dimensional fiber structures.

2.4.1 Python

Although languages like C++ or Fortran have a performance advantage compared to Python, due to being a compiled language, projects can be implemented, and concepts iterated, more rapidly in Python. Additionally, the Python language benefits from a large, enthusiastic, open source community. Many performance advantages of compiled languages disappear when Python's utility as a "glue" language is considered as well. Functions requiring high performance can be implemented in lower level, more efficient languages, compiled and executed through Python allowing for both performance and implementation speed. Many useful packages have been developed, tested, and vetted by the community and are available for open source use with broad, if any license for derivative use. The concepts developed in this thesis are implemented using Python and two such open source packages.

2.4.2   NumPy

NumPy provides a stable, efficient, array structure and various functions for computing with arrays. In addition to standard arithmetic element-wise and matrix operations, NumPy includes an assortment of linear algebra, array creation and manipulation, random number generation, and convenience functions. This simulation relies heavily on the array structure, and breadth of available functionality to implement both the individual steps and connecting framework described in the following chapters.

2.4.3   SciPy

While NumPy is sufficient, and more efficient for most array operations, the SciPy package provides a large set of scientific computing functionality including N-d interpolation, root-finding, numerical optimization, and statistical routines not implemented by NumPy. Most established scientific computing algorithms, excluding machine learning and neural network, are implemented in SciPy or are otherwise easily implemented using SciPy functions. While NumPy provides the structure for the simulation, efficient optimization and interpolation are performed with SciPy functions.

CHAPTER 3
PROBABILISTIC REPRESENTATION OF CHAOTIC FLUID DYNAMICS

While substantial insight is found through deterministic models, the mathematical machinery describing particle fluid interaction inherently leads to sensitive dependence and chaotic dynamics. Furthermore, the input fibers cannot be described except in terms of randomly distributed variables. That is, the results of any one simulation represent a single sample from a much richer underlying distribution. This is problematic for deterministic simulations because it requires substantial repetition of potentially computationally expensive experiments to elucidate the true diversity of the output space. Rather than duplicate the dynamic process we seek to create a representation of the probability measure of the final placements.

3.1 Derivation of Probability Measure

Consider a particle suspended in a fluid above an evenly spaced $N \times N$ grid, depicted in Figure 3.1. Let the particle be located randomly with equal probability anywhere in the fluid. Now imagine that the initial volume of fluid is allowed to flow through the grid. Then the probability, $p_{i,j}$, that the particle will pass through grid element i,j is proportional to the flow through that element. The probability the particle will pass through one of the elements on the grid is given by:

$$\sum_i^{N_i} \sum_j^{N_j} p_{i,j} = 1 \tag{3.1}$$

Denote the flow of fluid through the element i,j by $J_{i,j}$. Then the probability a particle is found in a given grid element is:

$$p_{i,j} = \frac{J_{i,j}}{\sum_{n=1}^{N} \sum_{m=1}^{N} J_{n,m}} \tag{3.2}$$

11
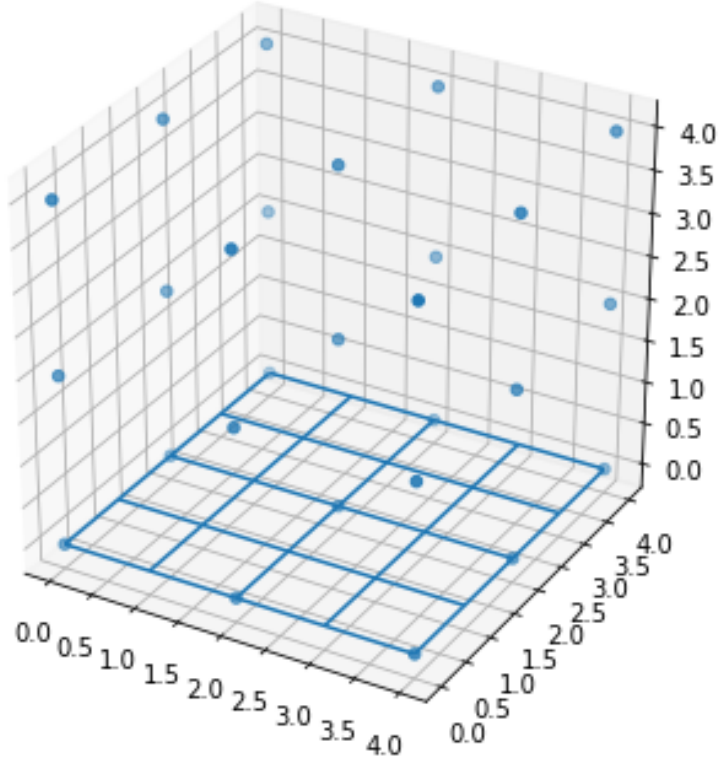
Figure 3.1. Particles Suspended Uniformly Above a Grid

This construction implies that the distribution of placement locations follows the multinomial distribution with density function:

$$P\left(\mathbf{x}|n,\mathbf{p}\right) = \frac{n!}{\prod_{n=1}^{N}\prod_{m=1}^{N}x_{n,m}}\prod_{n=1}^{N}\prod_{m=1}^{N}p_{n,m}^{x_{n,m}} \qquad (3.3)$$

With the probabilities $\mathbf{p}$ as defined above. For a single particle $n = 1$ and the result is extended to multiple independent particles by allowing $n \geq 1$.

The result is used to simulate packed particle structure formation by assigning each grid element a height $H_{i,j}$ and allowing each particle to add to the height at their respective elements. The flow at each element is approximated by Darcy's Law:

$$Flux = \frac{Driving\ Force}{Resistance} = J_{i,j} = \frac{\Delta P}{\alpha\ H_{i,j}} \qquad (3.4)$$

12
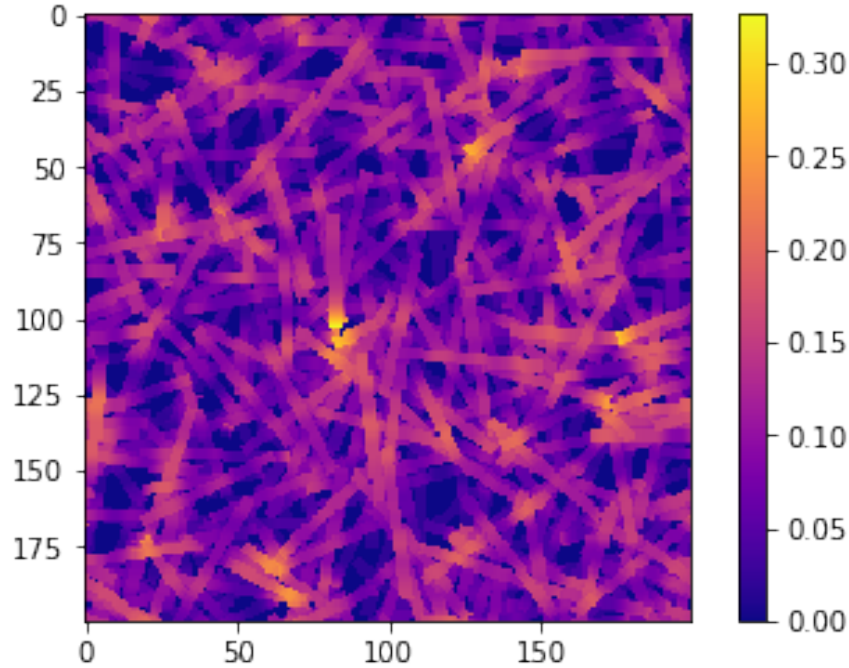
Figure 3.2. Example Packed Particle Structure

Where $J_{i,j}$ is the flux, $R_{i,j}$ is the resistance, and the driving force is pressure change, $\Delta P_{i,j}$. Resistance is approximated as $R_{i,j} = \alpha \ H_{i,j}$ where α is cake resistance. Substituting the expression for $J_{i,j}$ into the expression for $p_{i,j}$ yields:

$$p_{i,j} = \frac{1}{H_{i,j} \ \sum_{n=1}^{N} \sum_{m=1}^{N} \frac{1}{H_{n,m}}} \tag{3.5}$$

With the heights of the topography initialized to any positive number to avoid undefined probabilities when $H_{i,j} = 0$. For simplicity let $H_{i,j}^{0} = 1$. Figures 3.2 depicts an example of a packed particle topography and Figure 3.3 shows the corresponding placement probabilities computed by equation 3.5.

For large particles, covering many grid elements, the placement location of the center of the particle is determined by sampling the above distribution with $n = 1$.

While this representation is not dynamic in the continuous sense; the placement of fibers one at a time determines a "fiber clock", and the evolution of the topography is a recursive, discrete, stochastic system.

13
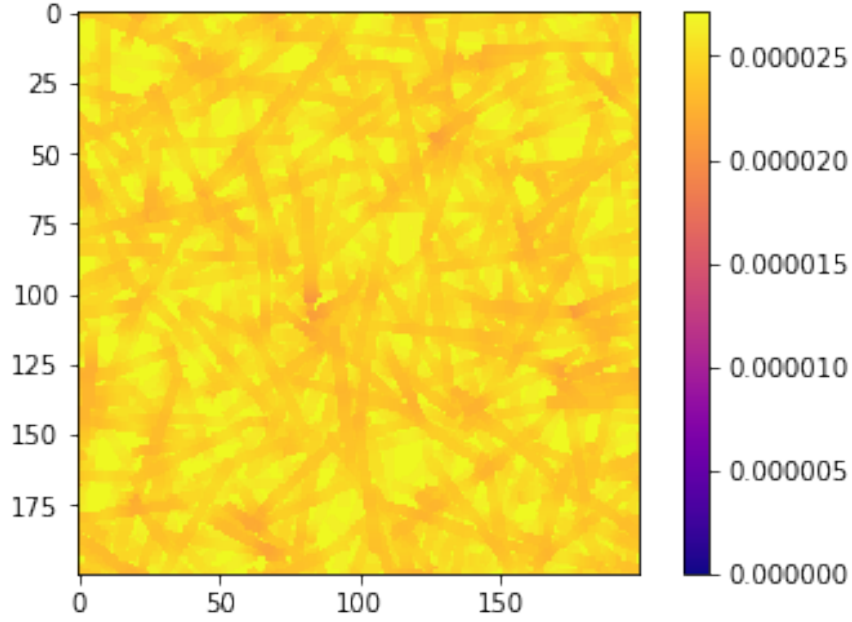
Figure 3.3. Placement Probability Topography

3.2 Simultaneous Placement of Many Small Particles

As mentioned in the previous section, the multinomial distribution can be used to determine the placement location of many small (all dimensions less than the grid size), independent particles. If there is an average of λ small particles per large particle, then the number of small particles, n, placed between each large change to the topography, and corresponding probabilities, can be approximated by the Poisson distribution with parameter λ. That is, for each large particle placed n small particles may also be placed, where n is a random, Poisson distributed, integer. Then, the multinomial distribution can be used to determine the placement of each of the n small particles simultaneously. The Poisson density function is given by:

$$P\left(n \mid \lambda\right) = \frac{\lambda^n\, e^{-\lambda}}{n!} \tag{3.6}$$

Particles assigned to the same element are treated as being locally continuous so that the height change at the element is given by the sum of the volume contributions of the

14

small particles divided by the area of the element. If the volume contributions of the small particles are exponentially distributed with mean particle volume, $\bar{v}$, then the particle volume density function is given by:

$$f(v_p) = \frac{1}{\bar{v}} e^{\frac{v_p}{\bar{v}}} \tag{3.7}$$

The sum of identically exponentially distributed variables is gamma distributed, with shape parameter equal to the number of exponential variables, n, in the sum and scale equal to $\bar{v}$ with the density function:

$$f\left(\sum v_p\right) = \frac{1}{\Gamma(n)\bar{v}^n} \left(\sum v_p\right)^{n-1} e^{\frac{\sum v_p}{\bar{v}}} \tag{3.8}$$

By treating small particles as locally continuous and calculating their placement contributions, thousands or millions of small particles can be incorporated into the structure with minimal additional computation.

CHAPTER 4

MINIMIZATION OF FIBER POTENTIAL ENERGY

In this model the final conformation of the fiber to the existing structure topography is determined, for a given placement location, by minimizing the potential energy of the fiber at that location.

4.1   Derivation of Minimization Problem

In the xz plane, where x, z correspond to the fiber's axial dimension and the vertical dimension, consider a twice differentiable function $z(x)$ representing the profile of the maximum height of the bottom surface of the fiber and a piece-wise function $h(x)$ representing the height profile of the existing structure's surface (in the fiber's frame of reference) where $z(x) \geq h(x)$.

Let the fiber be represented by a sequence N of elastically connected point masses equally spaced in x with height profile $z(x)$ suspended above a topography with height profile $h(x)$.

Then the potential energy of each point $i = 1, 2, ...N$ is the sum of the gravitational and elastic potential energies at the point.

Gravitational potential energy, PE_i^G, of each point relative to the topography surface is:

$$PE_i^G = \rho \, g \, (z_i - h_i) \tag{4.1}$$

Where ρ is the density of the fiber and g is the gravitational acceleration constant. Additional potentials (Such as pressure) can be applied similarly.

Elastic Potential Energy at each point, PE_i^E, is proportional to the squared curvature of the height profile at that point. The finite difference method to approximate curvature is given by:
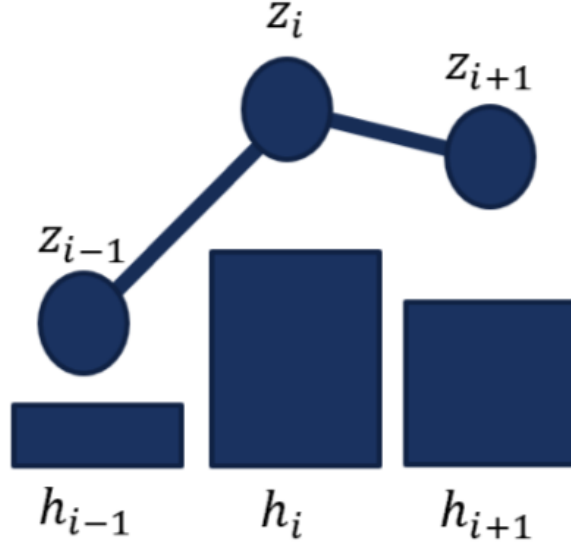
Figure 4.1. Schematic of Model Fiber

$$z_i'' = \frac{2z_i - z_{i-1} - z_{i+1}}{\Delta x^2} \tag{4.2}$$

Then the elastic potential energy at each point of the fiber is:

$$PE_i^E = \frac{k}{2\,\Delta x^4}\left(2z_i - z_{i-1} - z_{i+1}\right)^2 \tag{4.3}$$

Boundary conditions are handled by specifying $z_0 = 2z_1 - z_2$ and $z_{N+1} = 2z_N - z_{N+1}$ where the points z_0 and z_{N+1} are only invoked to compute the curvature at z_1 and z_N and do not represent elements of the fiber.

Then the total potential energy of a fiber:

$$PE^T \propto \sum_{i=1}^{N}(PE_i^G + PE_i^E) = \rho\,g\sum_{i=1}^{N}z_i - \rho\,g\sum_{i=1}^{N}h_i + \frac{k}{2\Delta x^4}\sum_{i=1}^{N}(2z_i - z_{i-1} - z_{i+1})^2 \tag{4.4}$$

$$\implies PE^T \propto f(\mathbf{z}) = \sum_{i=1}^{N}z_i + \frac{\sigma}{\Delta x^4}\sum_{i=1}^{N}(2z_i - z_{i-1} - z_{i+1})^2 \tag{4.5}$$

Where $f(\mathbf{z})$ is the objective function for minimization and $\sigma = \frac{k}{2\,\rho\,g}$ represents the stiffness of the fiber.
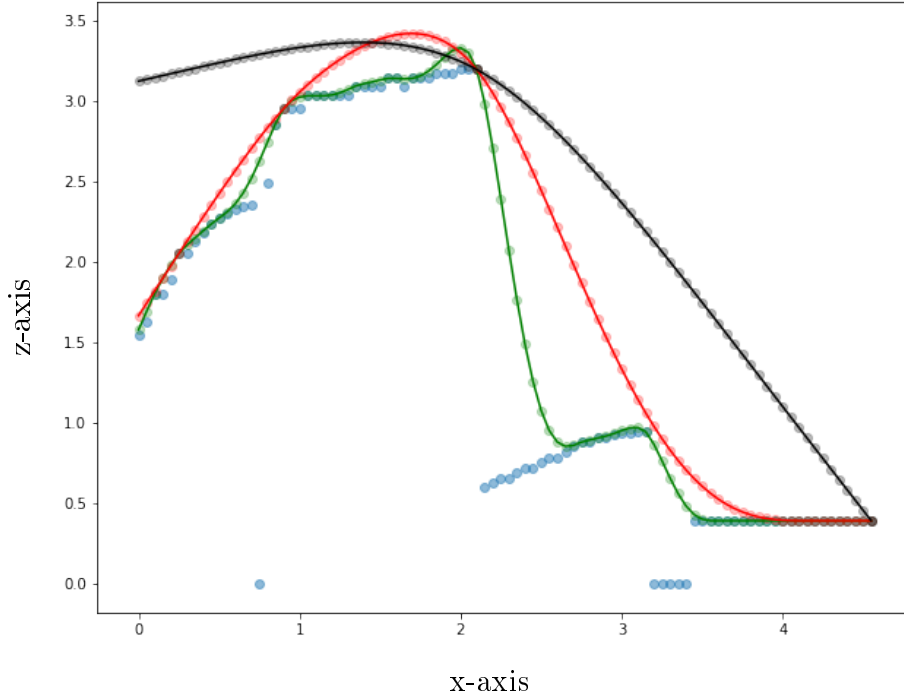
Figure 4.2. Optimized Fibers of Various, Increasing Stiffness (Green, Red, and Black) Suspended Over a Slice of the Topography (Blue).

To summarize, fiber placement is the minimization of $f(\mathbf{z})$ where $\mathbf{z}$ is bounded from below by $\mathbf{h}$. The vector $\mathbf{z}$ represents the true height profile $z(x)$ evaluated at $\mathbf{x}$ where $\mathbf{x}$ is a vector of N equally spaced elements along the particle axis. Similarly, $\mathbf{h} = h(\mathbf{x})$, where $h(x)$ is the extant topography below the fiber.

The cost function $f(\mathbf{z})$ is the sum of only convex terms so is convex. Furthermore, because each element z_i can be any value greater than or equal to h_i for all elements i, the feasible set is also convex, so any minimum is the global minimum.

Practically, the bounded minimization is performed in the Python SciPy package [16] using the minimize function with the 'L-BFGS-B' [19] method. Providing the Jacobian of the cost function, $\nabla f(\mathbf{z})$, rather than relying on internal approximations, substantially improves performance and guarantees convergence to the global minimum. Figure 4.2 shows the optimization solution for three different, increasing, stiffness green, red, and black, placed onto a slice of the topography in blue.

The jth element of the Jacobian is given by:

$$\frac{\partial}{\partial z_j} f(\mathbf{z}) = \frac{\partial}{\partial z_j} \sum_{i=1}^{N} z_i + \frac{\partial}{\partial z_j} \frac{\sigma}{\Delta x^4} \sum_{i=1}^{N} (2z_i - z_{i-1} - z_{i+1})^2 \qquad (4.6)$$

For $j = 3, 4, ... N - 2$

$$= 1 + \frac{\sigma}{\Delta x^4} \frac{\partial}{\partial z_j} \sum_{j-1}^{j+1} (2z_i - z_{i-1} - z_{i+1})^2$$

$$= 1 + \frac{\sigma}{\Delta x^4} \frac{\partial}{\partial z_j} \left((2z_{j-1} - z_{j-2} - z_j)^2 + (2z_j - z_{j-1} - z_{j+1})^2 + (2z_{j+1} - z_j - z_{j+2})^2 \right)$$

$$\frac{\partial}{\partial z_j} f(\mathbf{z}) = 1 + \frac{\sigma}{\Delta x^4} \left(2z_{j-2} - 8z_{j-1} + 12z_j - 8z_{j+1} + 2z_{j+1} \right) \qquad (4.7)$$

Similarly, applying the boundary conditions, $z_0 = 2z_1 - z_2$ and $z_{N+1} = 2z_N - z_{N-1}$, yields:

$$\frac{\partial f(\mathbf{z})}{\partial z_1} = 1 + \frac{\sigma}{\Delta x^4} \left(2z_1 - 4z_2 + 2z_3 \right) \qquad (4.8)$$

$$\frac{\partial f(\mathbf{z})}{\partial z_2} = 1 + \frac{\sigma}{\Delta x^4} \left(-4z_1 + 10z_2 - 8z_3 + 2z_4 \right) \qquad (4.9)$$

and,

$$\frac{\partial f(\mathbf{z})}{\partial z_N} = 1 + \frac{\sigma}{\Delta x^4} \left(2z_{N-2} - 4z_{N-1} + 2z_N \right) \qquad (4.10)$$

$$\frac{\partial f(\mathbf{z})}{\partial z_{N-1}} = 1 + \frac{\sigma}{\Delta x^4} \left(2z_{N-3} - 8z_{N-2} + 10z_{N-1} - 4z_N \right) \qquad (4.11)$$

Expressing the problem in matrix form to reduce computational cost:

$$f(\mathbf{z}) = \sum (\mathbf{z}) + \frac{\sigma}{\Delta x^4} \sum (\mathbf{A} \, \mathbf{z})^2 \qquad (4.12)$$

and

19

$$\nabla f(\mathbf{z}) = 1 + \frac{\sigma}{\Delta x^4} \mathbf{B} \, \mathbf{z} \tag{4.13}$$

With:

$$A = \begin{bmatrix} 0 & 0 & 0 & 0 & 0 & \ldots & 0 \\ -1 & 2 & -1 & 0 & 0 & \ldots & 0 \\ 0 & -1 & 2 & -1 & 0 & \ldots & 0 \\ & & \ddots & \ddots & \ddots & \ddots & \\ \ldots & 0 & -1 & 2 & -1 & 0 & \ldots \\ & & \ddots & \ddots & \ddots & \ddots & \\ 0 & \ldots & 0 & -1 & 2 & -1 & 0 \\ 0 & \ldots & 0 & 0 & -1 & 2 & -1 \\ 0 & \ldots & 0 & 0 & 0 & 0 & 0 \end{bmatrix} \tag{4.14}$$

and:

$$B = \begin{bmatrix} 2 & -4 & 2 & 0 & 0 & 0 & 0 & \ldots & 0 \\ -4 & 10 & -8 & 2 & 0 & 0 & 0 & \ldots & 0 \\ 2 & -8 & 12 & -8 & 2 & 0 & 0 & \ldots & 0 \\ & & \ddots & \ddots & \ddots & \ddots & & & \\ \ldots & 0 & 2 & -8 & 12 & -8 & 2 & 0 & \ldots \\ & & \ddots & \ddots & \ddots & \ddots & & & \\ 0 & \ldots & 0 & 0 & 2 & -8 & 12 & -8 & 2 \\ 0 & \ldots & 0 & 0 & 0 & 2 & -8 & 10 & -4 \\ 0 & \ldots & 0 & 0 & 0 & 0 & 2 & -4 & 2 \end{bmatrix} \tag{4.15}$$

4.2 Limiting Behavior as Stiffness Increases

Let $\mathbf{z}_{min}$ be the solution to the optimization problem described previously, and let $z_{min}(x)$ be the corresponding height profile of the bottom of the fiber.

As stiffness increases infinitely the curvature term of the cost function must tend to zero in order to maintain balance with the height term:

$$\sigma \to \infty \implies \sum (\mathbf{A} \, \mathbf{z}_{min})^2 \to 0 \tag{4.16}$$

Since

$$\mathbf{A} \, \mathbf{z}_{min} \approx z''_{min}(\mathbf{x}) \implies z'_{min}(\mathbf{x}) = constant \tag{4.17}$$

At the limit, where the fiber is perfectly stiff, the slope is constant and the line $z(x)$ is specified for all points in x with only two degrees of freedom representing the slope and intercept.

Let $z_1 = z(x_1)$ and let $z_N = z(x_N)$

Then

$$z(x) = \frac{z_N - z_1}{x_N - x_1}(x - x_1) + z_1 \tag{4.18}$$

$$\implies f(\mathbf{z}) = \sum \mathbf{z} = \frac{z_N - z_1}{x_N - x_1} \sum (x - x_1) + \sum z_1 \tag{4.19}$$

let $\bar{x} = \frac{1}{N} \sum \mathbf{x}$ and let $\bar{z} = \frac{1}{N} \sum \mathbf{z}$

$$\implies \bar{z} = \frac{z_N - z_1}{x_N - x_1}(\bar{x} - x_1) + z_1 = \frac{1}{2}(z_N + z_1) \tag{4.20}$$

Minimizing $\sum \mathbf{z}$ is then equivalent to minimizing $\bar{z}$, which is equivalent to minimizing $g(z_1, z_N) = z_1 + z_N$.

Since the inequality $\mathbf{z} \geq \mathbf{h}$ must still be satisfied, the problem becomes a constrained optimization problem. Constraints are expressed in matrix form:

$$\mathbf{X} \begin{bmatrix} z_N \\ z_1 \end{bmatrix} - \mathbf{h} \geq 0 \tag{4.21}$$
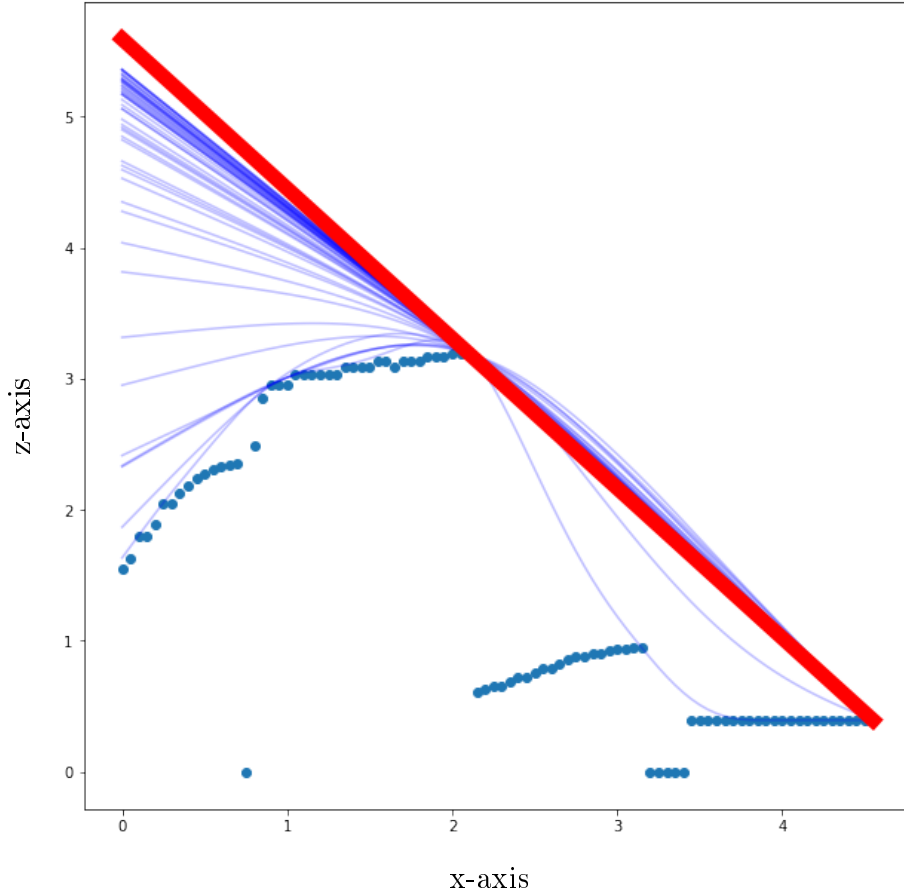
Where:

Figure 4.3. Fibers of Increasing Stiffness (Blue) and Perfectly Stiff Fiber (Red)

$$\mathbf{X} = \begin{bmatrix} 0 & 1 \\ \frac{x_2 - x_1}{x_N - x_1} & \left(1 - \frac{x_2 - x_1}{x_N - x_1}\right) \\ \dots & \dots \\ \frac{x_i - x_1}{x_N - x_1} & \left(1 - \frac{x_i - x_1}{x_N - x_1}\right) \\ \dots & \dots \\ \frac{x_{N-1} - x_1}{x_N - x_1} & \left(1 - \frac{x_{N-1} - x_1}{x_N - x_1}\right) \\ 1 & 0 \end{bmatrix} \quad (4.22)$$

The problem is solved in Python with the minimize function from SciPy optimization package using the "SLSQP" method [20]. The limiting case is depicted in Figure 4.3.
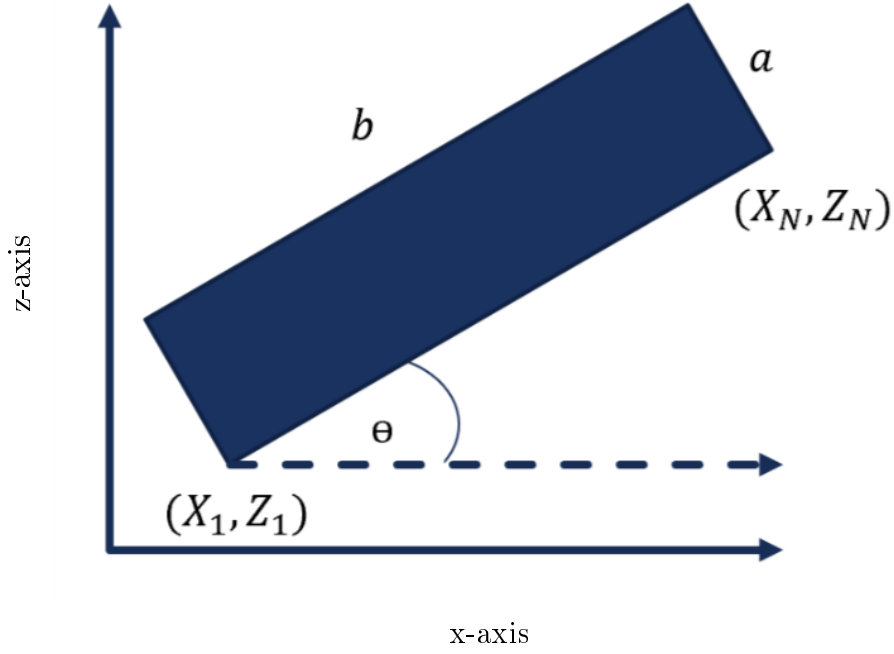
Figure 4.4. Schematic of Fixed Length Model Fiber

4.3 Stiff Fibers of Fixed Length

While the potential energy minimization method and limiting behavior described in the previous sections are convenient abstractions of real particles, they are not entirely realistic. Consider the perfectly stiff case; as $Z_n - Z_1$ is increased the fiber becomes elongated with the magnitude of elongation dependent on the random topography beneath the fiber. The elongation increases without convergence as more fibers are added to the structure. By the previous construction the fiber spans all x points of the below topography. In order to mitigate the elongation, the length of the fiber is fixed at b. The changes in z and x from one end to the other of a fiber rotated θ degrees relative to the topography plane are then:

$$\Delta Z = b \; sin \; \theta \tag{4.23}$$

$$\Delta X = b \; cos \; \theta \tag{4.24}$$

Let (X_1, Z_1), (X_N, Z_N) represent the coordinates of each end of the fiber related by:

23

$$Z_N = Z_1 + \Delta Z \tag{4.25}$$

$$X_N = X_1 + \Delta X \tag{4.26}$$

The previous cost function in terms of Z_1 and θ is then:

$$g(Z_1, \theta) = Z_1 + Z_N(Z_1, \theta) = 2 \, Z_1 + b \, sin \, \theta \tag{4.27}$$

The height profile of the bottom of the fiber is defined for all elements in x by:

$$Z_{bot}(x) = \begin{cases} tan(\theta)(x - X_1) + Z_1 & X_1 \le x \le X_N, \\ h(x) & Elsewhere \end{cases} \tag{4.28}$$

Where $Z_{bot}(\mathbf{x}) - h(\mathbf{x}) \ge 0$. For $X_1 \le x \le X_N$, the piecewise height profile represents the particle's bottom surface. Otherwise $Z_{bot}(x)$ is set equal to $h(x)$ to satisfy constraints at points that do not represent the particle.

Fixing the fiber length means that, as the fiber is rotated from horizontal to vertical, it's image onto the topography below is changed. This changes the constraints of the problem in random way, consistent with the random topography below. When the fiber is horizontal more points are included in the specification of constraints, when the fiber is vertical, less points are included. Because the topography can be multimodal, circumstances arise where the feasible set of placements of an initially vertical fiber is disjoint from the feasible set of placements of an initially horizontal fiber. For example, consider a hole large enough for a vertically oriented fiber to pass through but small enough block horizontally orient fibers. As a result, the solution space to the minimization problem is no longer convex. Furthermore, if the particle is rotated 90° in either direction the bottom surface of the particle is defined by a single point $(x_{bot}, Z_{bot}(x_{bot}))$. If $x_{bot} \notin \mathbf{x}$, then g is unbounded from below. Introducing height profiles for all sides of the particle and setting the grid size less than the smallest dimension particle size ensures the final placement is realistically constrained by the topography. The top, left, and, right height
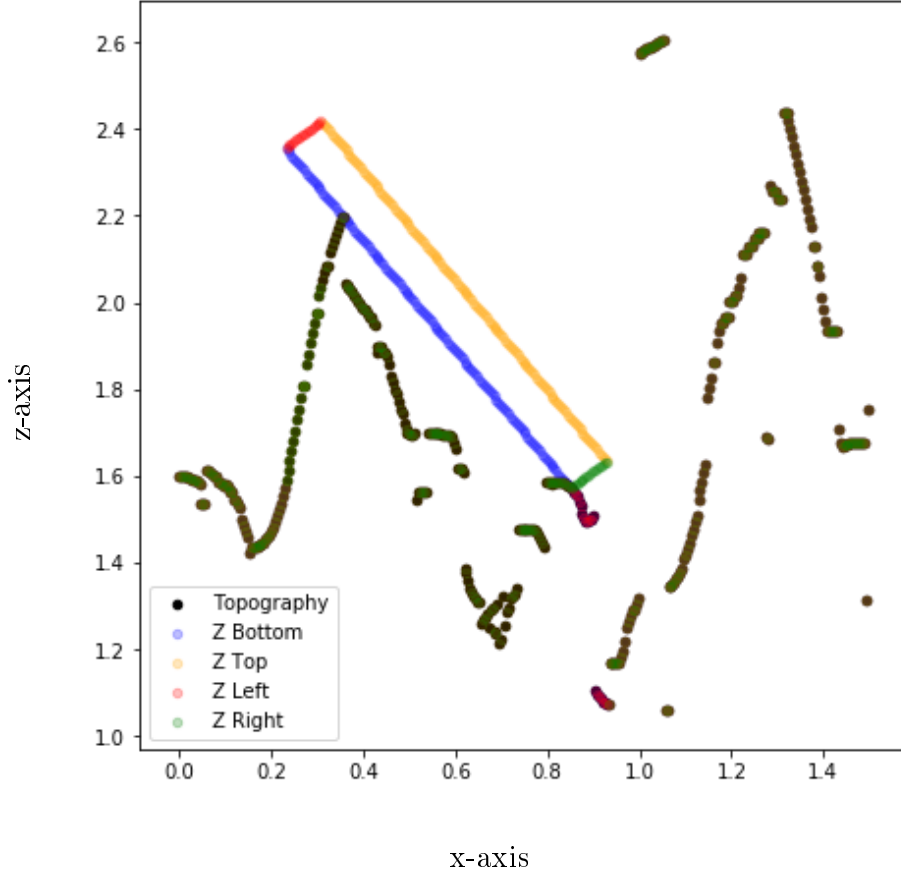
Figure 4.5. Z Profiles for Each Side of the Fiber Used for Constrained Optimization

profiles are given below. An depiction of the height profiles of all four sides plus the

underlying topography is shown in Figure 4.5.

$$Z_{top}(x) = \begin{cases} tan(\theta)(x - X_1 - \Delta x) + Z_1 + \Delta z & X_1 + \Delta x \le x \le X_N + \Delta x, \\ h(x) & Elsewhere \end{cases} \quad (4.29)$$

$$Z_{left}(x) = \begin{cases} \frac{-1}{tan(\theta)}(x - X_1) + Z_1 & min(X_1, X_1 + \Delta x) \le x \le max(X_1, X_1 + \Delta x), \\ h(x) & Elsewhere \end{cases}$$

$$(4.30)$$

$$Z_{right}(x) = \begin{cases} \frac{-1}{tan(\theta)}(x - X_N) + Z_N & min(X_N, X_N + \Delta x) \leq x \leq max(X_N, X_N + \Delta x), \\ h(x) & Elsewhere \end{cases}$$

<div align="right">(4.31)</div>

Where:

$$\Delta z = a\ cos\left(\frac{\pi}{2} + \theta\right) \tag{4.32}$$

$$\Delta x = a\ sin\left(\frac{\pi}{2} + \theta\right) \tag{4.33}$$

And:

$$(Z_{top}(\mathbf{x}),\ Z_{left}(\mathbf{x}),\ Z_{right}(\mathbf{x})) - h(\mathbf{x})\ \geq\ 0 \tag{4.34}$$

Additionally, X_1 is allowed to vary and the following constraints are applied:

$$X_1 \geq 0, \tag{4.35}$$

$$x_{max} \geq X_N, \tag{4.36}$$

$$X_1 + \Delta x \geq 0, \tag{4.37}$$

$$x_{max} \geq X_N + \Delta x \tag{4.38}$$

Since the problem is no longer convex, a local solution is obtained, again using the SciPy "SLSQP" method, with an initial guess determined by centering the fiber along the line defined by the solution to the stiff-convex problem defined in the previous section.

CHAPTER 5
DESCRIPTION OF PACKING ALGORITHM

The probability measure and optimization techniques described in previous chapters allows for the rapid determination of fiber placement location subject to chaotic fluid dynamics and optimization of the final fiber conformation for individual fibers given an existing topography. This chapter describes the connecting framework used to evolve the topography from an initial state to the final structure.

5.1 Definition of Topography

The first step to the simulation is to define an empty topography. For simplicity consider only square topographies. Given a side length and number of elements per side L and N, a topography is generated represented by 3 $N \times N$ matrices for the coordinates (X, Y, H), representing a grid of $N \times N$ points on the surface of the simulated paper. That is each i corresponds to a value $X_{i,j=1...N}$, and j corresponds to a value $Y_{i=1..N,j}$, and $H_{i,j}$ represents the height at each $i, j \implies X, Y$ pair. Each $H_{i,j}$ is initialized to 1. The topography is updated with the placement of each macro-fiber and the placement of fibers is dependent only on the topography in its most current state. A depiction of the topography grid is shown in Figure 5.1.
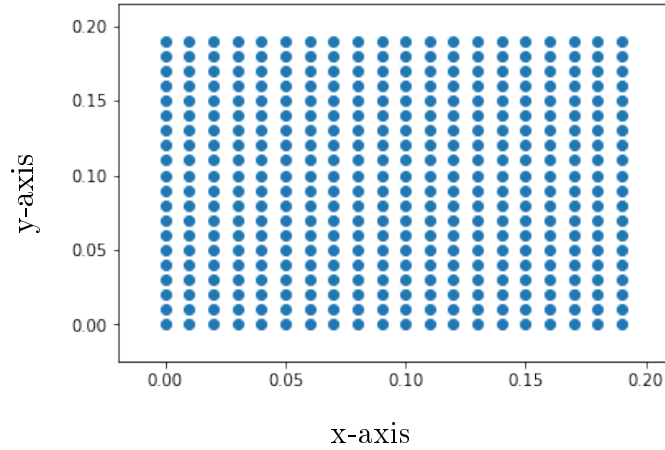
Figure 5.1. Topography Mesh Grid

5.2 Definition of Filtration Media

Although an empty initial topography is compatible with the simulation methodology, it may occasionally (for example in a study of the retention of fine particles or screen fouling) be desirable to study the effect of different filtration substrates on sheet or processing properties. In these cases, the topography is initialized with H set to an initial thickness greater than 1 at corresponding elements. For example, a simple screen geometry is shown in Figure 5.2. Given any initial topography, fiber placement proceeds as normal.
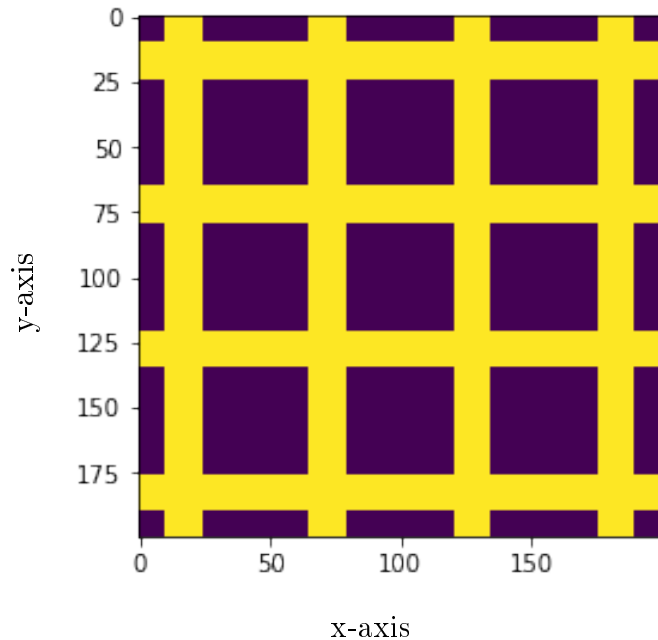
Figure 5.2. Simple Screen Geometry

5.3   Selection and Extraction of Slice

Following the specification of an initial topography, the algorithm proceeds placing fibers one at a time by selecting the placement location of a fiber, determining its final conformation, updating the topography, and repeating with a new fiber until the desired number of fibers is placed. The topography of a packed fiber structure is depicted in Figure fig:filtercake-1.
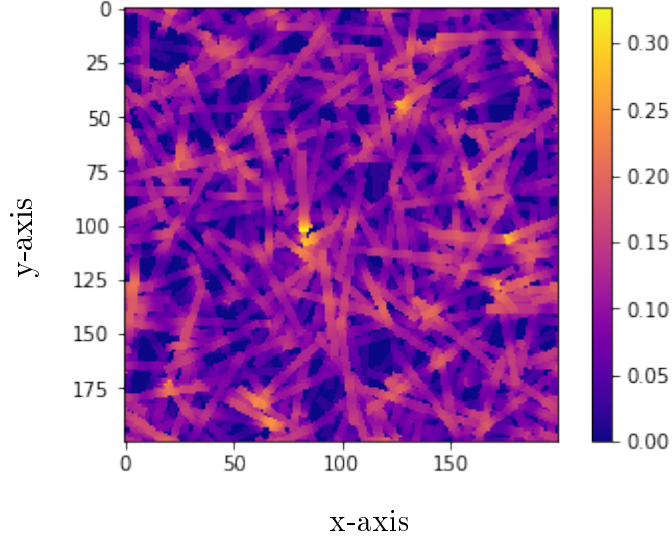
Figure 5.3. Example Packed Structure Topography

For each fiber, the next step is to locate and extract a slice on which to place a fiber. Like the topography a fiber is represented by 3 matrices for the coordinates of the bottom surface of the particle. However, each i, j pair represent points in the particle frame of reference X_p, Y_p. The coordinates are transformed into the topography frame of reference using an affine transformation by:

$$A \times (vec(X_p), vec(Y_p), vec(Z_p))$$

With Z_p initialized to 1 where A is the matrix representing the affine transformation implied by the grid element sampled from the probability measure defined in chapter 2 and, for simplicity, a normally distributed angle of rotation, ϕ.

$$A = \begin{bmatrix} cos\phi & -sin\phi & \Delta x \\ sin\phi & cos\phi & \Delta y \\ 0 & 0 & 1 \end{bmatrix}$$

Figure 5.4 and Figure 5.5 depict the image of the fiber in the topography frame of reference and the corresponding slice of topography heights.
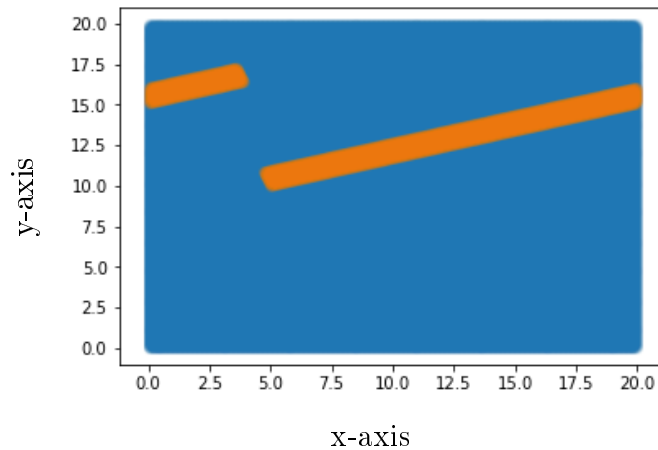
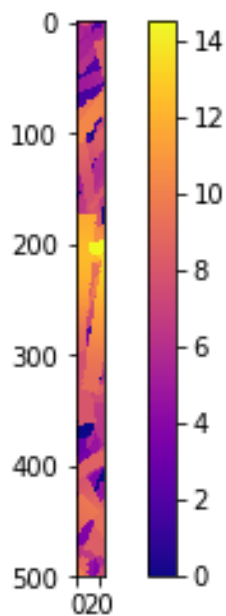Figure 5.4. Fiber Points in the Topography Frame of Reference

Figure 5.5. Extracted Slice

5.4 Placement of Particle

Once a slice is extracted the conformation of the fiber is determined by taking the maximum along the short axis of the slice and optimizing the placement of a fiber along the slice using a combination of the methods described above, depicted in Figure 5.6. First,

the solution to the limiting problem is found (thin blue line). This solution is used as a guess for the fixed length problem (orange points). Finally, the solution to the fixed length problem (green points) defines the domain used in the original minimization problem described for curved fibers (thin red lines). The first problem provides very good guess for a realistic solution to a local minimization of the fixed length problem. The fixed length problem is used to bound the elongation of fibers in the structure to an acceptable level.
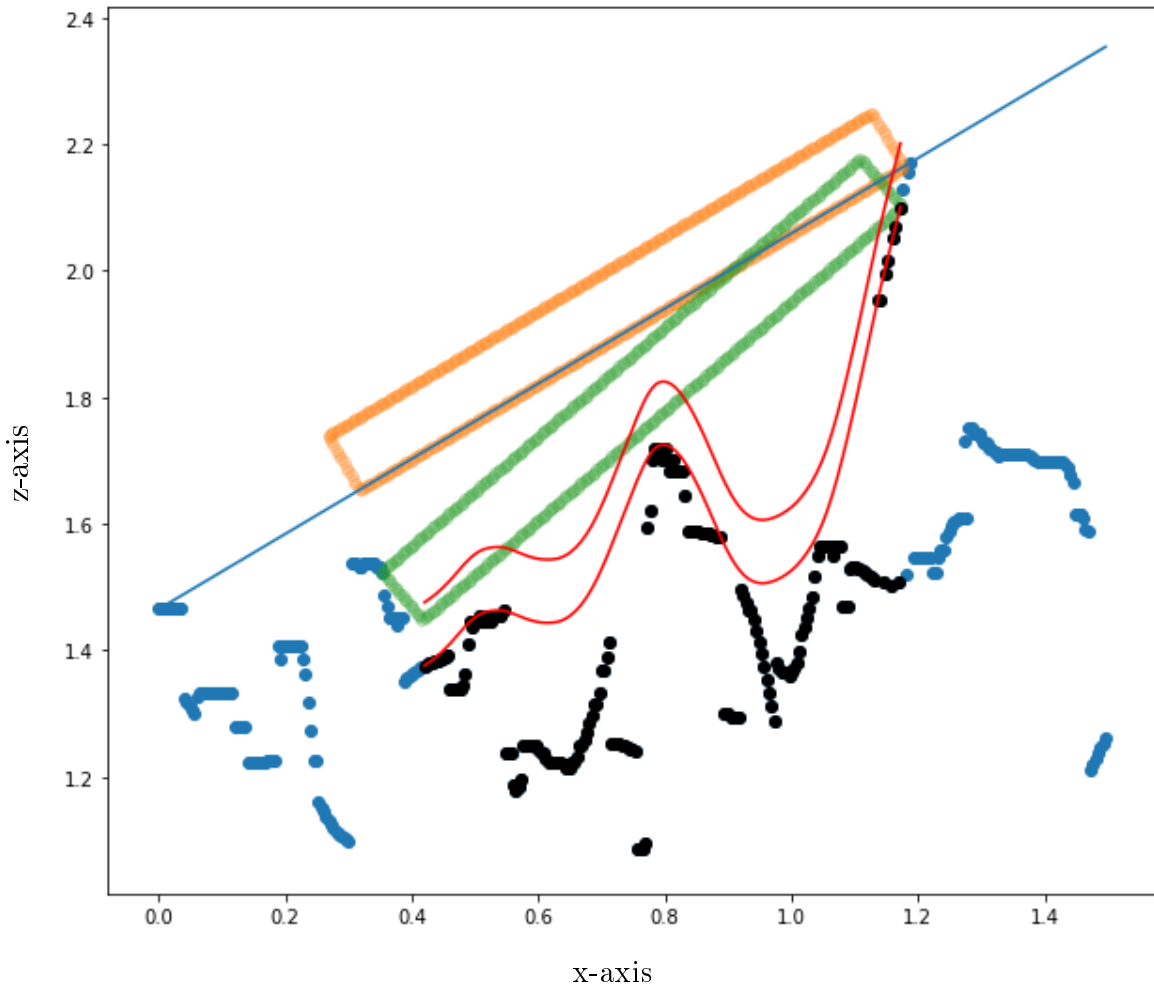

Figure 5.6. Optimization Process for Fiber Placement

After the solving for the curvature of the fiber at each point along its long axis the height along the short axis is set equal at each point. In order to place the fiber onto the current topography, the coordinates computed during the slice selection and extraction

step need to be digitized back to corresponding elements i, j in the topography grid. While this step seems trivial it results in nuisance perforations due to rounding errors that are difficult to remove with simple arithmetic and otherwise require an unacceptable increase in grid elements. Fortunately, the SciPy Package contains an implementation of the grey closing algorithm, as implemented in SciPy [16], which is used as a final step to fill in elements. The result of the operation for an example fiber is shown in Figure 5.7. Once the perforations are removed, the height of the topography is updated at corresponding points.
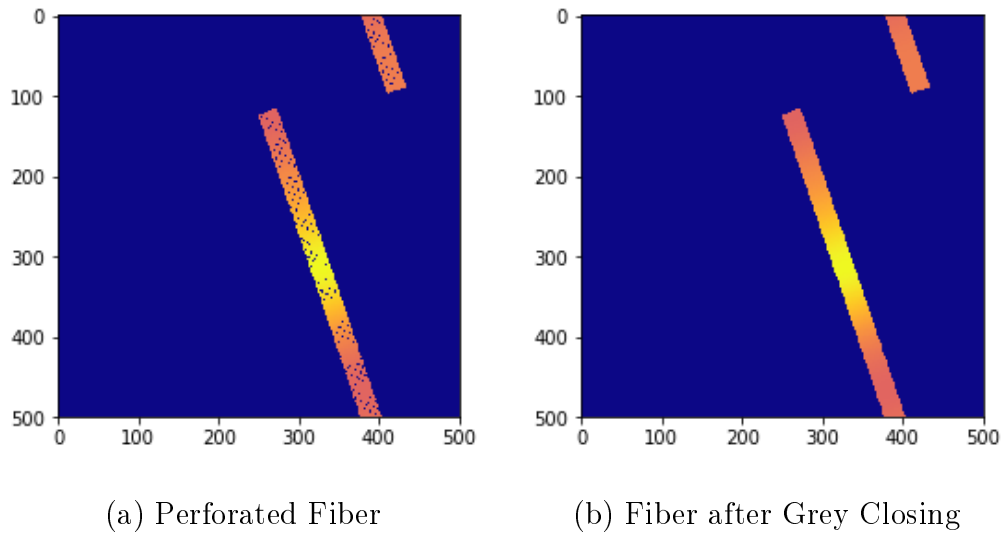

(a) Perforated Fiber   (b) Fiber after Grey Closing

Figure 5.7. Before and After Grey Closing Operation

CHAPTER 6
RESULTS AND DISCUSSION

6.1   Exploring Single Structure Results

Simulated structures are handled in two different ways, as a topography matrix, and as a list of points defining the fibers. Descriptive statistics and other quantities are computed from both as post processing steps. The topography can be visualized as a bitmap and the list of points can be rendered in a 3-d plotting software.

As described in previous chapters, the placement of each additional fiber is dependent on the existing structure only through the topography matrix. The topography is a collection of jointly randomly distributed surface heights. This is a natural and efficient representation of the structure and yields many useful results for direct analysis. The median height of the non-zero elements approximates the thickness of a corresponding lab-made handsheet, which can be used to approximate the bulk or density of the structure. The total area of topography elements with height equal to zero can be computed for later relation to permeability. The standard deviation of the height can be related to roughness and gloss. Generated topographies are visually realistic as seen in the topographies for low and high basis weights and flexible and stiff fibers shown in Figure 6.1. Corresponding histograms of the topography surface heights are shown in Figure 6.2.
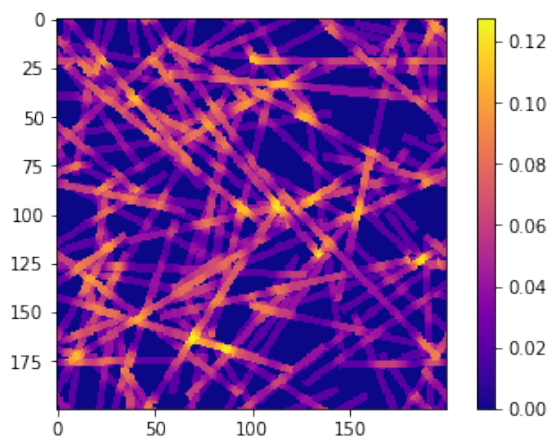
(a) Flexible Fibers Low Basis Weight
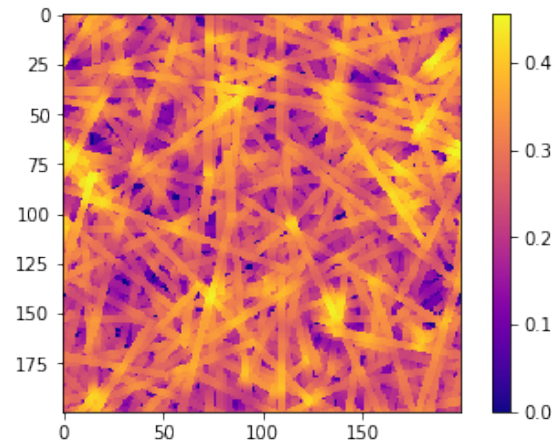
(b) Flexible Fibers High Basis Weight
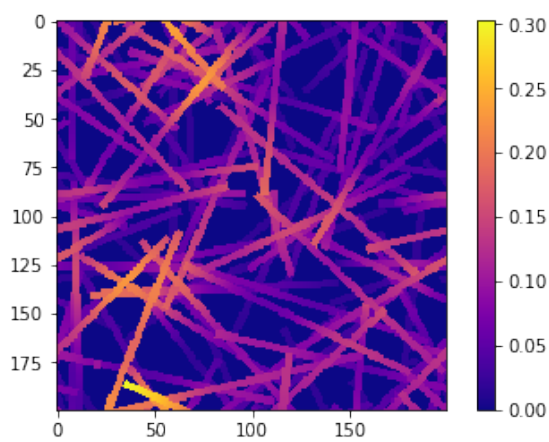
(c) Stiff Fibers Low Basis Weight

(d) Stiff Fibers High Basis Weight

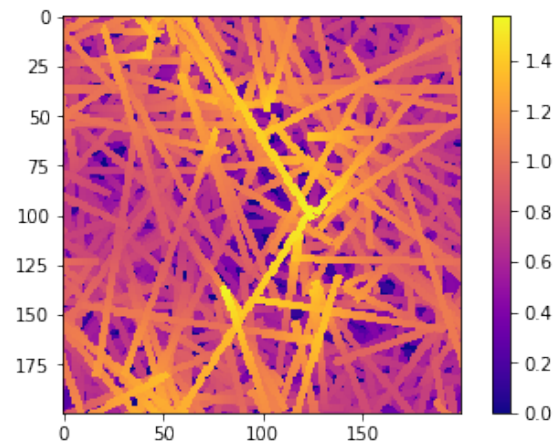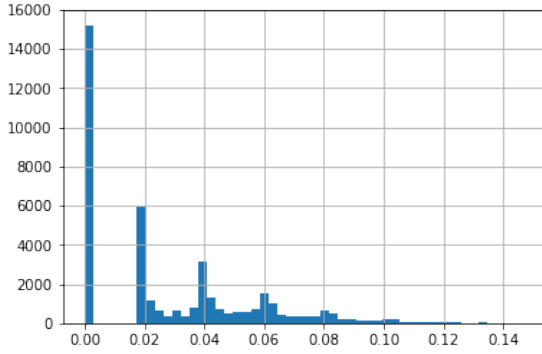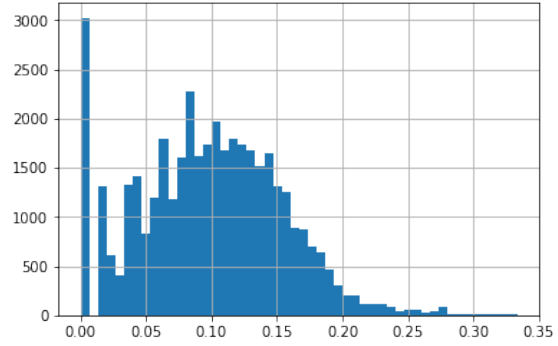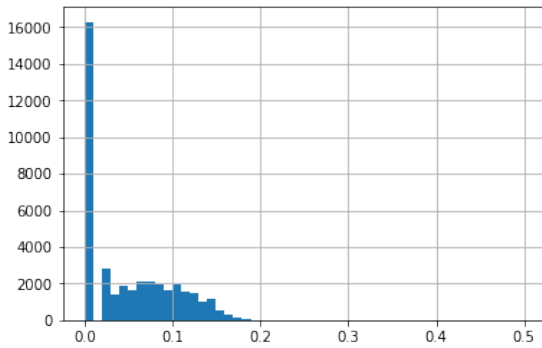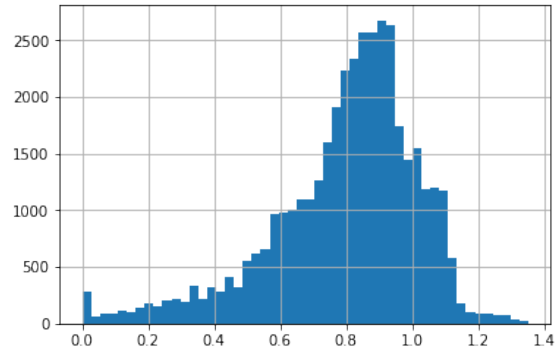Figure 6.1. Varying Basis Weight and Flexibility: Topographies

(a) Flexible Fibers Low Basis Weight

(b) Flexible Fibers High Basis Weight

(c) Stiff Fibers Low Basis Weight

(d) Stiff Fibers High Basis Weight

Figure 6.2. Varying Basis Weight and Flexibility: Surface Height Histograms

The topography matrix, though informative, is incomplete and many quantities need to be computed from a more complete structural representation. The height profile of the bottom and top surfaces, determined through the process described in chapters 3 and 4, is stored for each fiber, along with the height of the underlying topography, the curvature of the point. The detailed data allows for more descriptive analysis and visualization of the structure. As described in the original paper [9], pores, and associated pore size distributions, are difficult to define in closed form. Some work exists to define and quantify pore geometry of digital porous structures but such an analysis was not attempted during the completion of this project. Instead, each pore is defined as the vertical space between two fibers and is computed for each element of each fiber placed by taking the difference between the height of the bottom of the fiber and the height of the topography at each

fiber element. The spatial distribution of fiber to fiber connections for a low basis weight structure and the and spatial pore size distribution of a high basis weight structure are depicted in Figure 6.3.

(a)Low BW Fiber-Fiber Contacts, Top   (b)Low BW Fiber-Fiber Contacts, Side

(c) High BW Pore Distribution, Top   (d) High BW Pore Distribution, Side
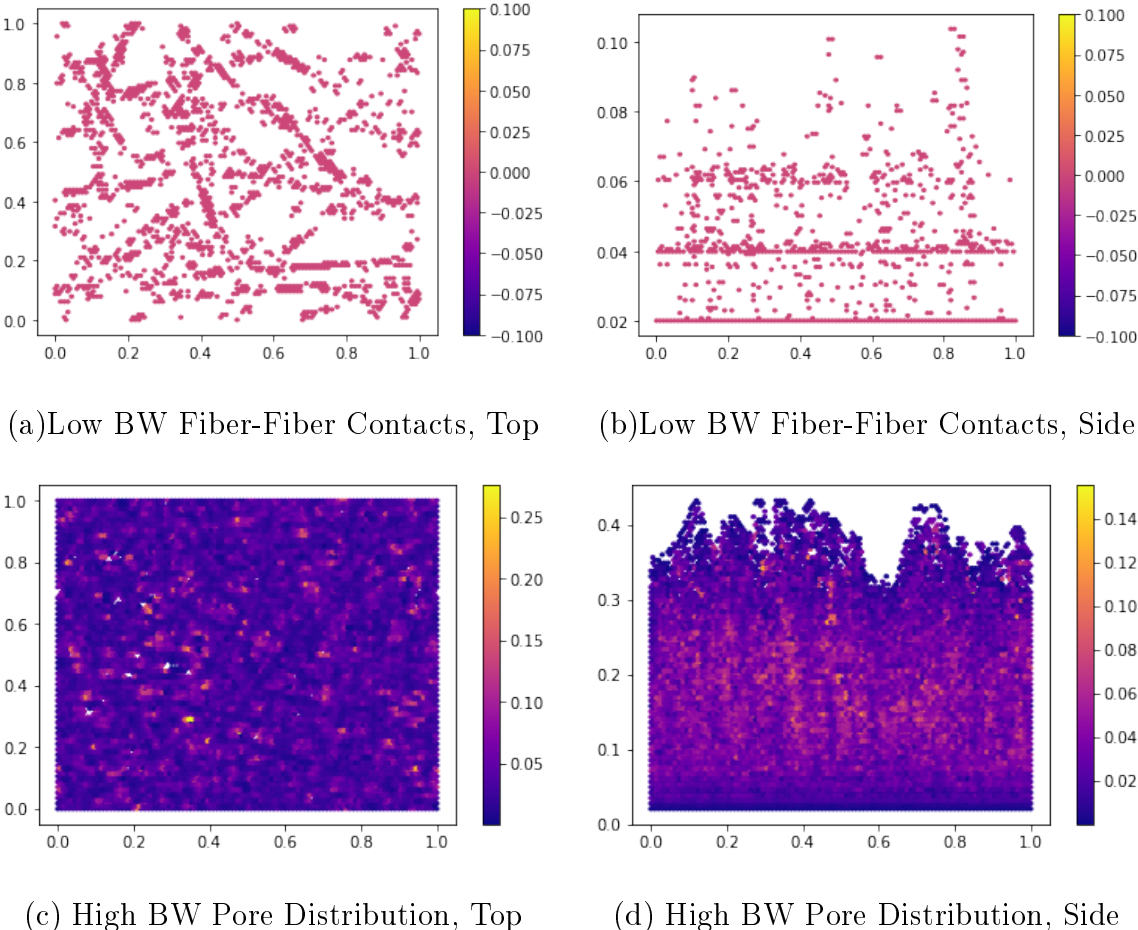
Figure 6.3. 2-Dimensional Depiction of 3-Dimensional Fiber Connection Network and Pore Network

6.2   Exploration of a Simple Fiber Space

Although visualization enhances intuition, which is necessary for model development, it cannot be used as a standalone prediction technique. Although the input space is designed to process a much wider range of fiber property distributions and mixtures, here, we restrict our attention to fibers with single valued properties and explore the baseline effect of basis weight, flexibility, fiber density, fiber length, and grid resolution. Similarly,

although the resulting structures are designed to provide broad perspective for future use in property prediction, we restrict our attention to the thickness of the structure since it is easily computed and can be directly compared with experimental measurements for calibration. Given the size of the available experimental space, more work is necessary to understand the full range of structures, available in the output space and their corresponding properties. Here, we share an informal calibration of the model to experimental thickness data.

Experimental data was collected over the summer of 2018 by Bangor High School STEM students Maddie Ahola and Reya Singh. Over one hundred handsheets of various compositions and basis weights were created based on the TAPPI procedure and tested for relevant properties, including thickness, tensile, gurley, mass, opacity, and color. Mixtures were composed of variable compositions of 2 of each of disintegrated bleached softwood pulp, disintegrated paper towels, and calcium carbonate.

The goal of this calibration is to determine the property range of a single pseudo-component that can provide good agreement with experimental results. As the composition of the handsheet is changed, the mean density, flexibility, and fiber length changes, as well as the fines composition. Fiber and fine size distributions and compositions as well as coarsity for the pulp and paper towel fibers were measured using a MorFi instrument. Although these measurements are generally representative of the source from which they were sampled, numerous challenges exist when sampling solid liquid systems. Primarily, due to the randomness of solids liquid systems, the sources sampled are not necessarily homogenous. When samples for MorFi analysis are prepared they are diluted several orders of magnitude to enable counting and analysis of each individual fiber. Particularly problematic during sample preparation is the settling of denser particles. For example, a sample might undergo 3 consecutive dilutions where 100 mL of pulp slurry at 1.2 percent solids is diluted to about 1 L, a 100 mL sample is taken, and the process repeated until a solids concentration of 0.002 percent is achieved, with the resulting solids

concentration at each step an order of magnitude lower than the first. Each time the sample is diluted to 1000 mL and the subsequent 100 mL sample is drawn from the top. This means that the most rapidly settling fibers will not end up in the sample measured by the MorFi. This is problematic as the MorFi yields an artificially low estimate of density. Given the likely presence of errors in the measurements, fiber properties should not be taken as fixed values and are varied within the range of measurements observed to best fit the data.

At this time, to avoid confounding results with many changing variables, we exclude fine particles, and the particle size distribution and simulate a single fiber with single valued properties. Unless otherwise specified, model input parameters are as follows. For all simulations a side length of 1 mm was used. Mean length weighted length, width and height, of fibers were determined using a MorFi instrument as $0.633mm$ and $0.02mm$ respectively. Fiber density was assumed similar to cellulose, $1.25 \ 10^{-3}$, which lies in the middle of the range of densities measured by the MorFi. The number of grid elements was held constant at 200 elements implying a resolution of $1/200$. The flexibility is not measured experimentally and must be determined by adjusting the model parameters so that results best fit the data. Flexibility is scaled by resolution so it can be compared consistently across grid sizes. A flexibility of $(1000mm^2)(Resolution^4 mm^{-4})$ yields a reasonable estimate of the lower limit of experimental data given the other parameters specified in this paragraph.

Four sets of simulated experiments are performed, varying basis weight and flexibility, varying basis weight and density, varying basis weight and fiber length, and varying basis weight and grid resolution, with the remaining variables specified as above. For each experiment 4 different basis weights, (mass per unit area) are considered, $(2.5, 6.67, 10.83, 15) \times 10^- 5 \frac{gm}{mm^2}$. For each basis weight, four conditions are simulated for each experiment as follows:

$$Flexibility : (1000, 214000, 427000, 640000)mm^2 \times Resolution^4 mm^{-4}$$
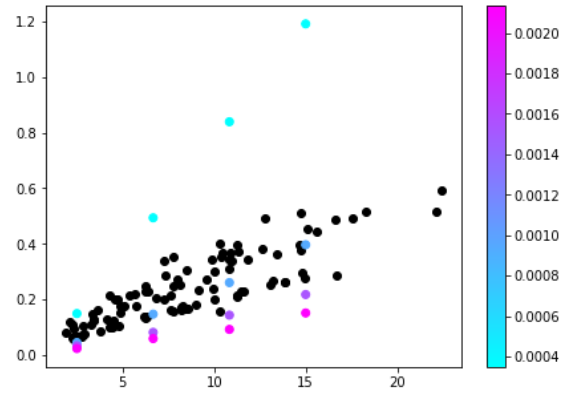
$$Density : (0.00035, 0.00095, 0.0015, 0.002)\frac{gm}{mm^3}$$
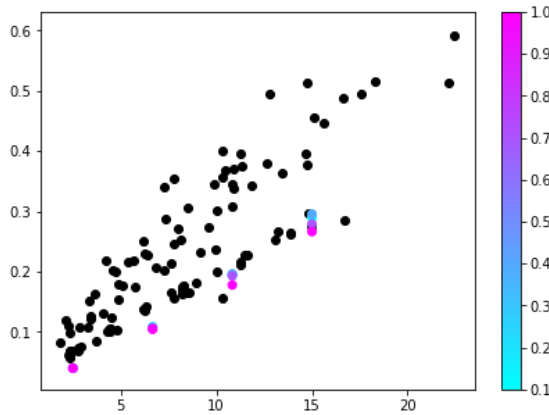
$$FiberLength : (0.1, 0.4, 0.7, 1.)mm$$

$$Resolution : (1/200, 1/400, 1/600, 1/800)mm$$
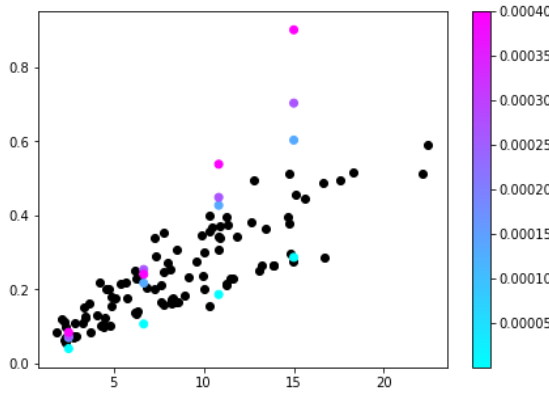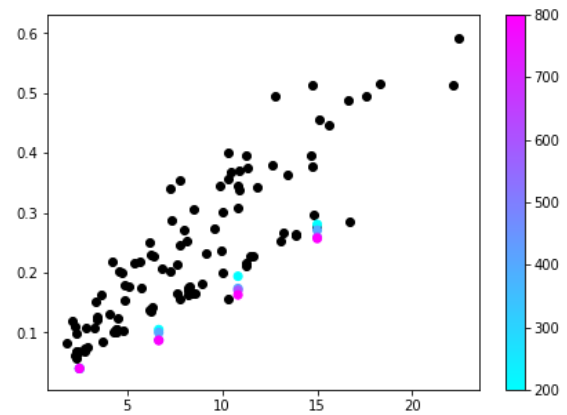
(a) Varying Flexibility
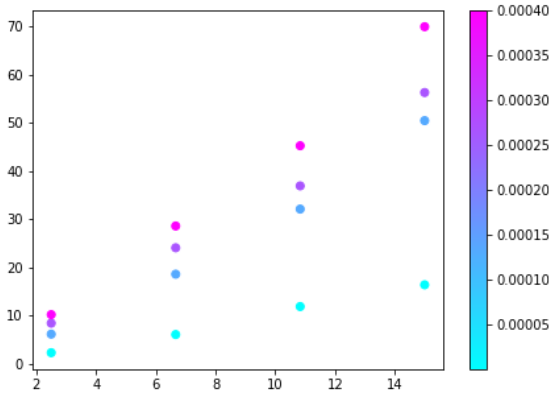
(b) Varying Density

(c)Varying Fiber Length

(d) Varying Grid Resolution

Figure 6.4. Median Thickness of Structure (mm) Vs Basis Weight ($10^{-5} \times \frac{gm}{mm^2}$), Colored by Secondary Variables

(a) Varying Flexibility
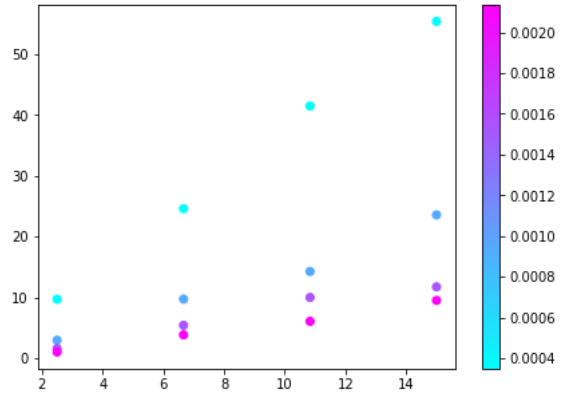
(b) Varying Density
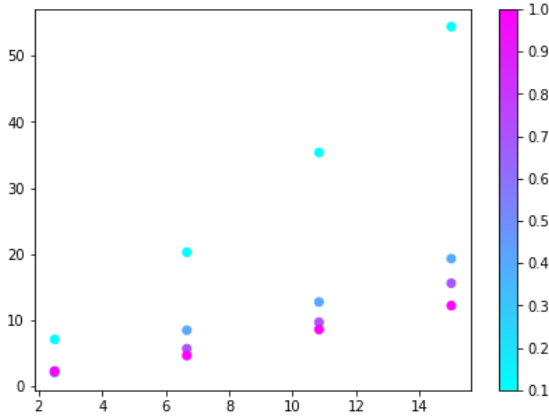
(c)Varying Fiber Length
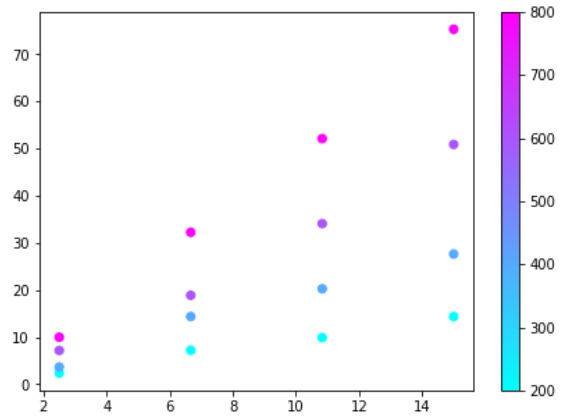
(d) Varying Grid Resolution

Figure 6.5. Structure Simulation Times ($Seconds$) Vs Basis Weight ($10^{-5} \times \frac{gm}{mm^2}$), Colored by Secondary Variables

From Figure 6.4, experimental thickness results fall within the range of the simulated results, using ranges estimated by MorFi and adjusting only the flexibility, demonstrating fiber input parameters can be calibrated for prediction purposes. Notable is the simulation speed. Richly detailed structures are generated on the order of a minute or less. Simulation times for the conditions represented in Figure 6.4 are shown in Figure 6.5.

Not surprisingly, basis weight, flexibility and density play large roles in determining the thickness of a sheet. The relationship with basis weight appears mostly linear, with

thickness approaching zero as basis weight approaches zero. Although not rigorously quantified here, the limiting behavior, when a single fiber remains is determined by the density of the fiber. Fibers with lower density occupy larger volume and therefore contributing more to the sheet thickness per basis weight than less dense fibers. Similar to basis weight, sheet thickness appears to vary linearly with fiber density. Flexibility changes the curvature of the change in basis weight versus sheet thickness. More analysis is necessary to understand this relationship.

Results show simulated structures are affected only modestly by the grid resolution. This means many screening studies can be performed at a coarse resolution, then, the most promising recipes can be studied in greater detail with finer resolution.

6.3 Repeatability

Using a fiber density of $0.00095\frac{gm}{mm^3}$, flexibility of $1000mm^2 \times Resolution^4 mm^{-4}$, Fiber length of $0.663mm$, resolution of $1/200mm$, 1000 simulations were executed at both $10^-5 \times 40gm/m^2$, and $10^-5 \times 120gm/m^2$. Histograms of the results are shown in Figure 6.6 with the high basis weight in blue and the low in orange. Notice that the variance increases as well as the mean with most quantities as basis weight is increased.
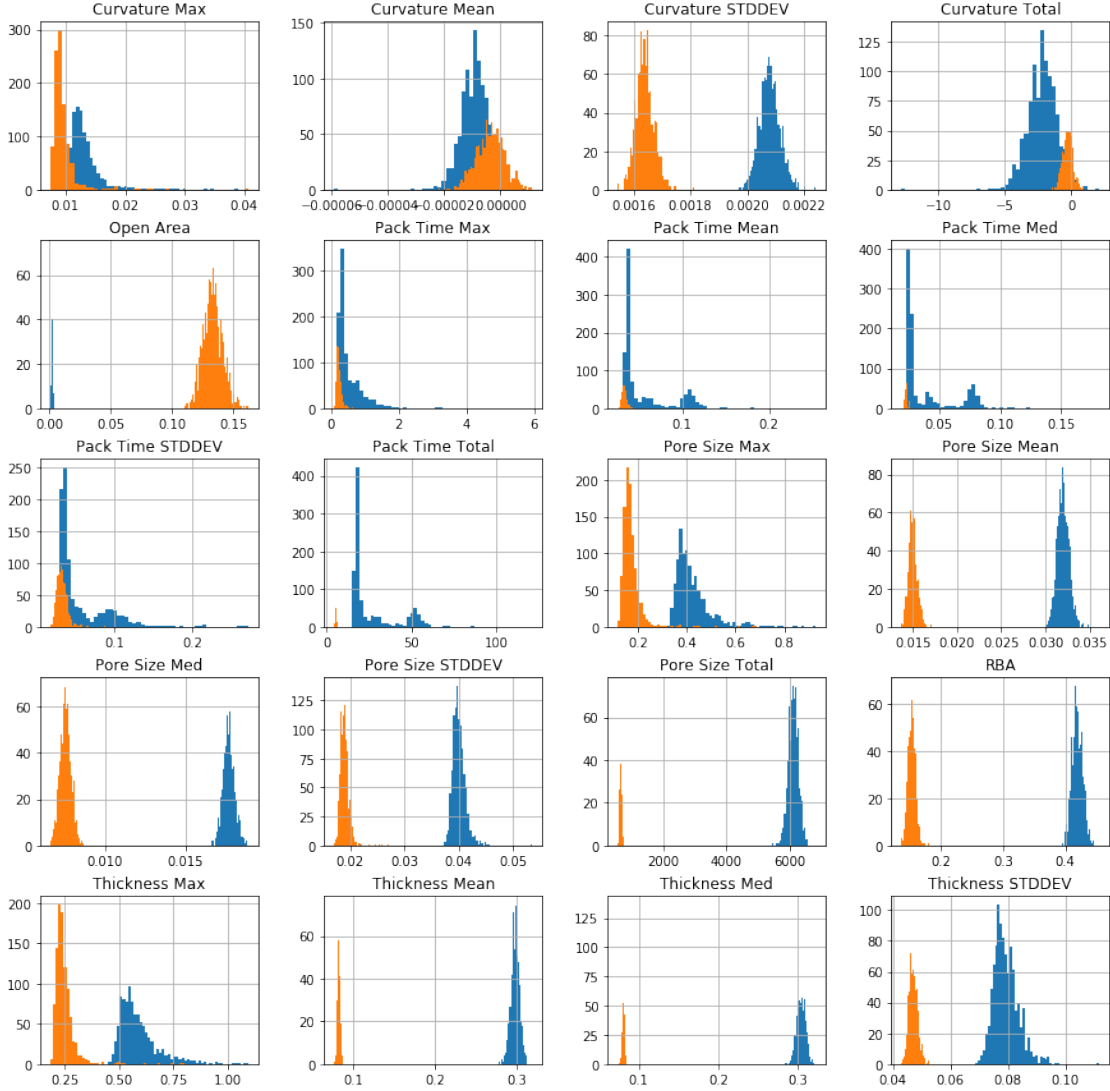
Figure 6.6. Repeated Simulations at the Same Conditions for High Basis Weight (Blue) and Low Basis Weight (Orange).

6.4 Elongation

As mentioned in chapter 4, one unrealistic effect of the model is the elongation experienced by each curved fiber. The elongation effect is effectively a map where the length of the placed fiber is determined by the input length, underlying topography, and stiffness.

$$b_{act} = f\left(b_{input} \mid \mathbf{h}, \sigma\right) \tag{6.1}$$

If the function mapping the desired length to the actual length could be determined, or at least approximated, then the relationship could be inverted allowing for the direct determination of the input length that yields the desired target length. Although we concede that the elongation effect is unrealistic, results show the elongation effect is minimal when the fiber is stiff and tolerable when flexible. Figure 6.7 and Figure 6.8 depict results for the elongation of flexible and stiff fibers respectively. The x-axis represents the length of a perfectly flexible fiber were it to be placed on the same slice, and the y-axis represents the length of the fiber actually place.d

Figure 6.7. Elongation of Flexible Fibers in a Single Structure

Figure 6.8. Elongation of Stiff Fibers in a Single Structure
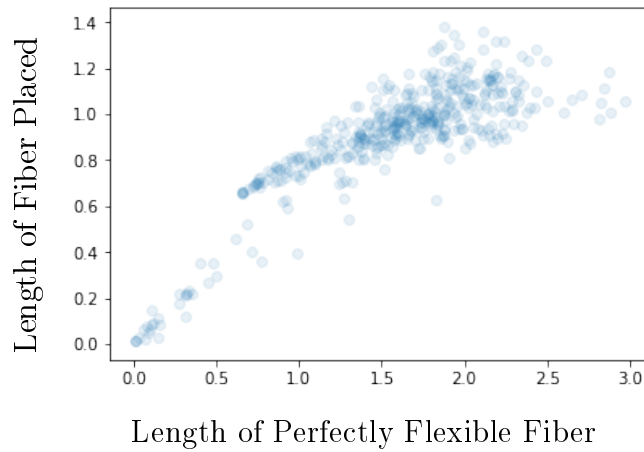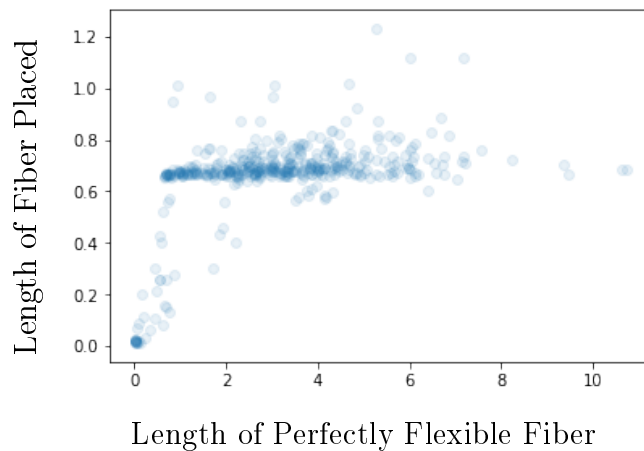
6.5 Effect of Probability Measure on Packing

As discussed in chapter 3, a novel probability measure is implemented to simulate the effect of filtration fluid dynamics during sheet formation. Initializing the height of the topography to different values changes the placement probability measure. When the initial heights are very low, close to the machine precision, the probability of a particle being placed on an empty grid cell is substantially higher than if the heights are initialized at one. As the initial height is increased, the probability measure governing particle placement becomes the uniform distribution. Figure 6.9 shows the effect of the initial height, and thus uniformity of the placements, on the sheet thickness. Although the median thickness of the structure changes little, the open area of the topography varies more substantially. Sheet open area versus log of initial height is shown in Figure 6.10. This suggests the effect on sheet formation is more subtle and likely affects the fiber and pore networks themselves. Although not studied here, it seems that changing the uniformity of the probability measure would most heavily influence the placement of small particles as large particles cross many elements of the sheet, negating an effect of changing probabilities.
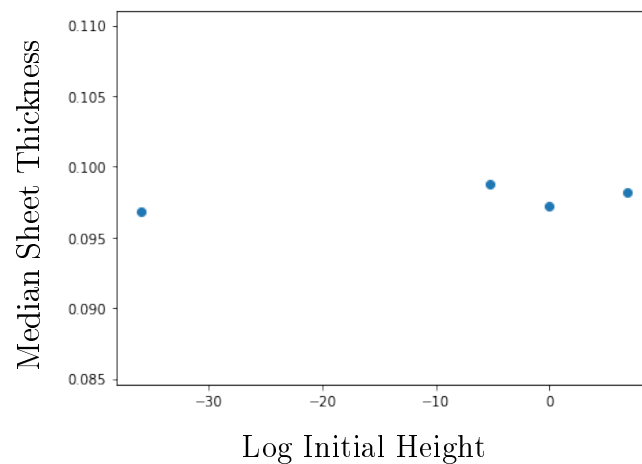

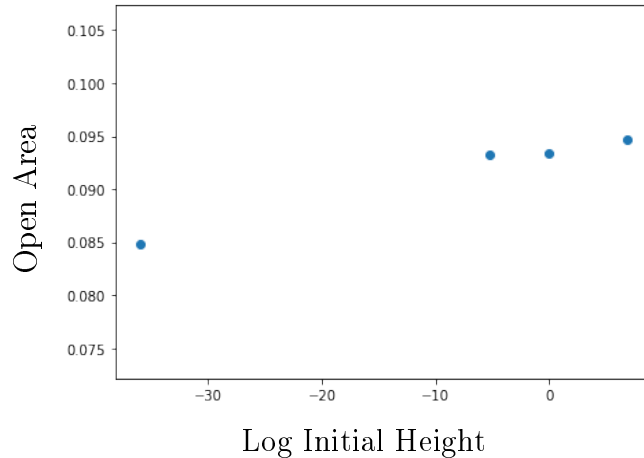Figure 6.9. Median Sheet Thickness Vs Log of Initial Height

Figure 6.10. Sheet Open Area Vs Log of Initial Height

The probability measure derived in chapter 3 represents a simple methodology by which to encode the result of a chaotic dynamical system in a compact form. Despite the simplicity of application, yet powerful descriptive capability, the model is an idealization of a real process. While we assume the flux through each element is dependent only on height, reality is more complex. While the model only considers flux orthogonal to the topography, the true flow characteristics are far more an-isotropic. That is, planar as well as orthogonal flows occur in the structure, and fluid moves through a tortuous path from the top of the sheet to the bottom. Consideration of such flows would add an order of magnitude of complexity to the model. One of the primary advantages and computational features is the storage of the entire process history using only the topography matrix. Because each step is only dependent on the surface heights, planar flows are not considered.

An additional non-ideality is the treatment of each element as essentially independent of its neighbors. Although the probability at each height is influenced by the rest of the structure through its relative proportion, it is not directly influenced by its neighbors. In real systems, flow at a point would be influenced by the height at its own element as well as neighboring elements. For example, consider an element with height 1 surrounded by points each with height $H > 1$ and a point with height 1 surrounded by points each with

height $H = 1$. In this situation, the element surrounded by neighbors with greater height represents a more restricted orifice for fluid flow than the open pore with open neighbors. If the total normalizing term is the same in both situations then, realistically, the flow should be higher at the open pore than at the restricted pore. To this end, numerous probability constructions could be derived that make use of neighboring information. The simplest strategy being the use of a uniform filter that takes the average of neighboring points. Despite the simplicity of this strategy it adds a new fitting parameter, the window size, to the model.

6.6 Demonstration of Model Capabilities

Although not fully explored at present, the simulation framework was designed to handle the full range of variability found in real paper inputs. Capabilities developed but not experimented with are shared here. Figures 6.11 to 6.15 depict in full three dimensional detail the proof of concept results for various simulated conditions representative of real paper.
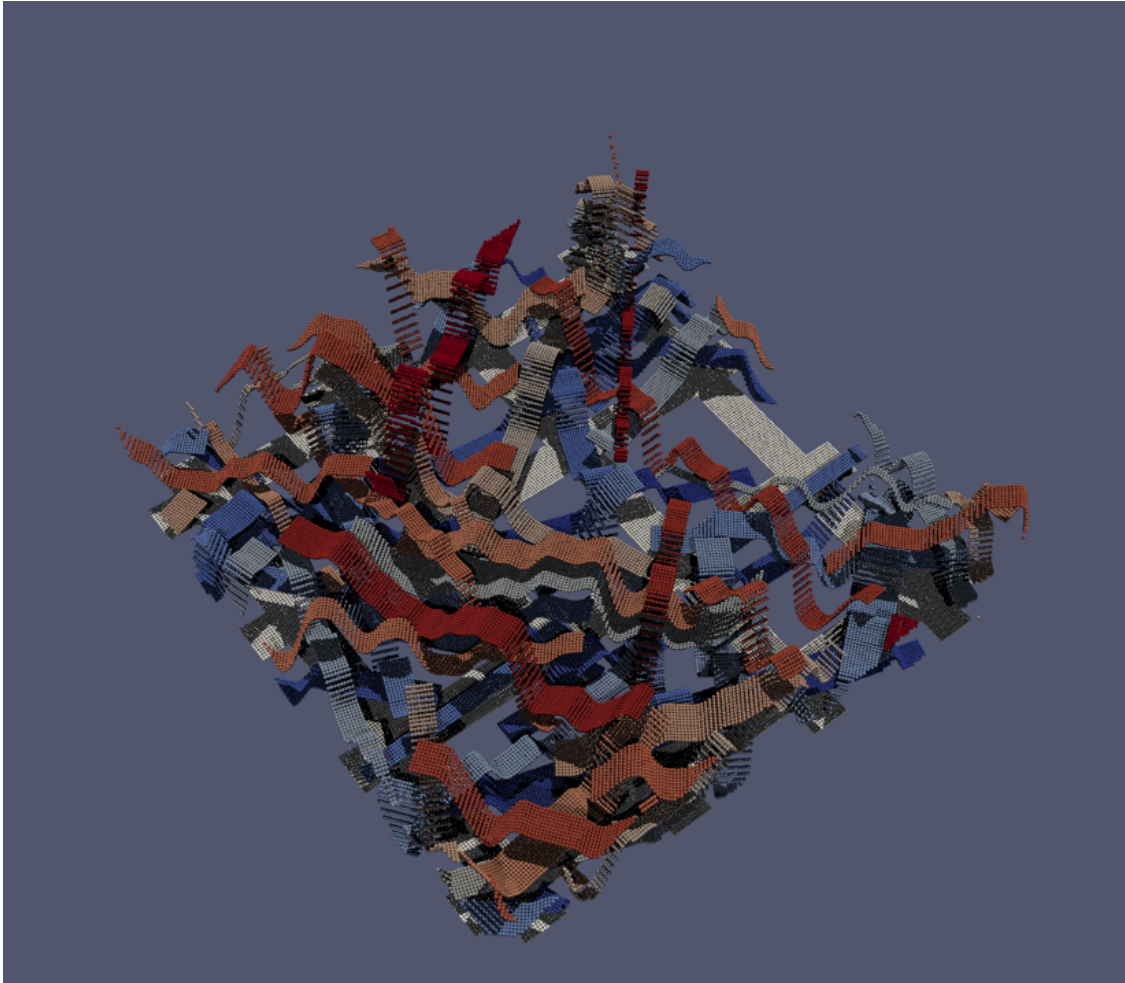
Figure 6.11. Random Fiber Dimensions. Real paper fibers do not have single valued properties and instead each fiber comes from a distribution of possible properties. The simulation allows for the placement of fibers with a large range of potential properties. Each individual fiber is stored as a row in a table and placed one at a time by the simulation. Any reasonable list of fibers can be provided, such as a random sample from a known probability distribution. A normal distribution is used to generate the sample of fibers pictured above.
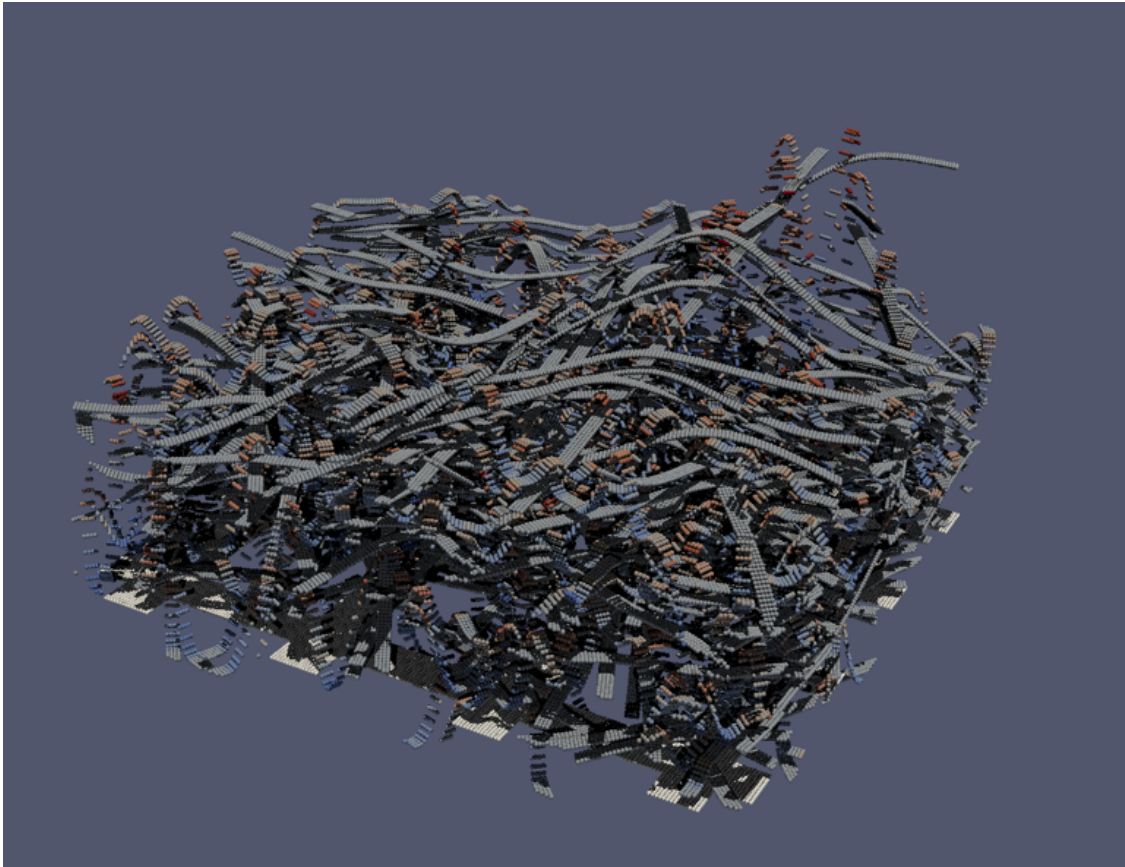
Figure 6.12. Mixed Fiber Types (Mixed Flexibilities Shown). Similar to randomly distributed fiber properties, fibers of different types can be mixed. This includes fibers with single valued properties, or two fiber types with different random physical property distributions. It is also possible to build different layers by using a previously generated topography as the starting point for a new structure.
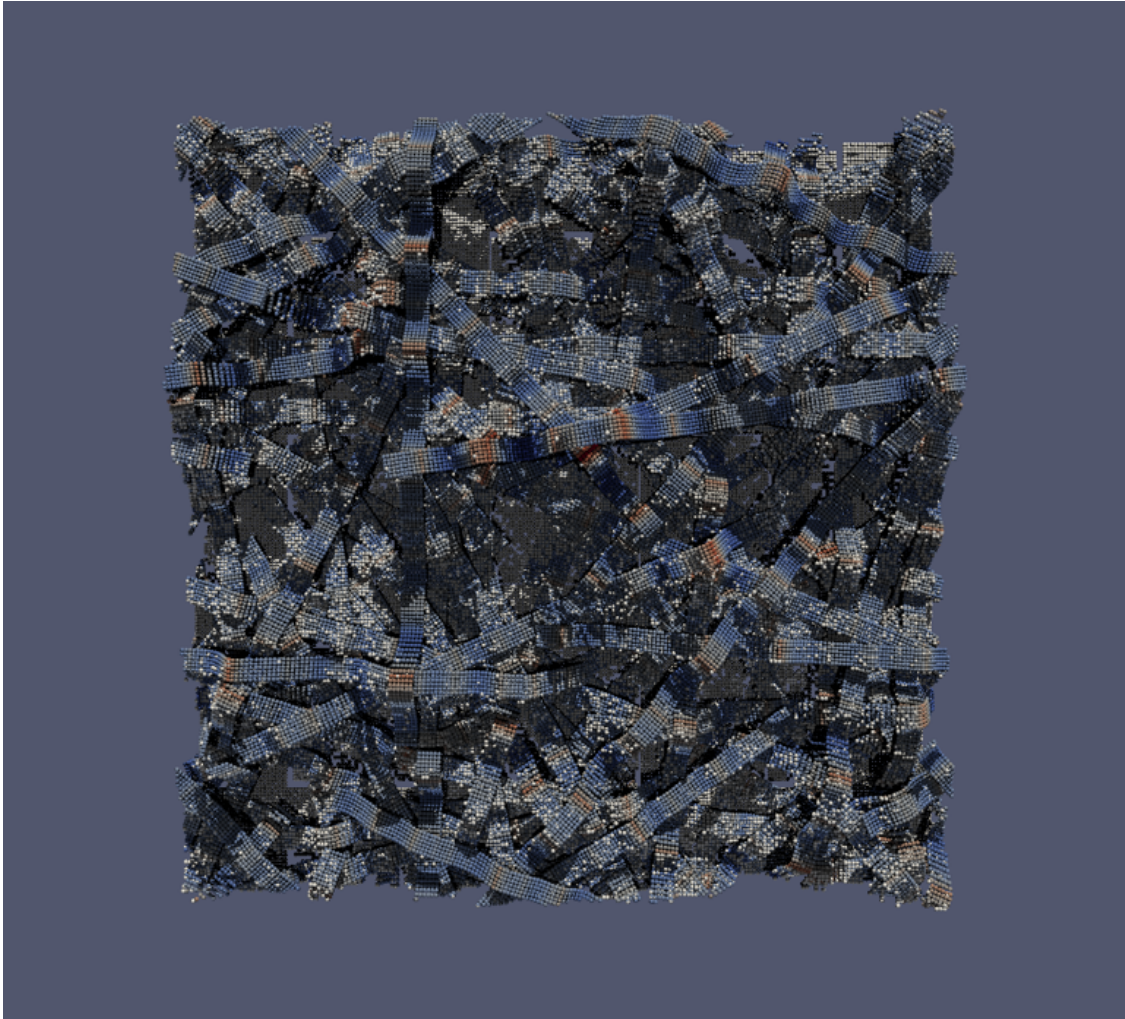
Figure 6.13. Fines, Top View. As described in chapter 3, the placement of many small particles, fines, can be accomplished simultaneously.
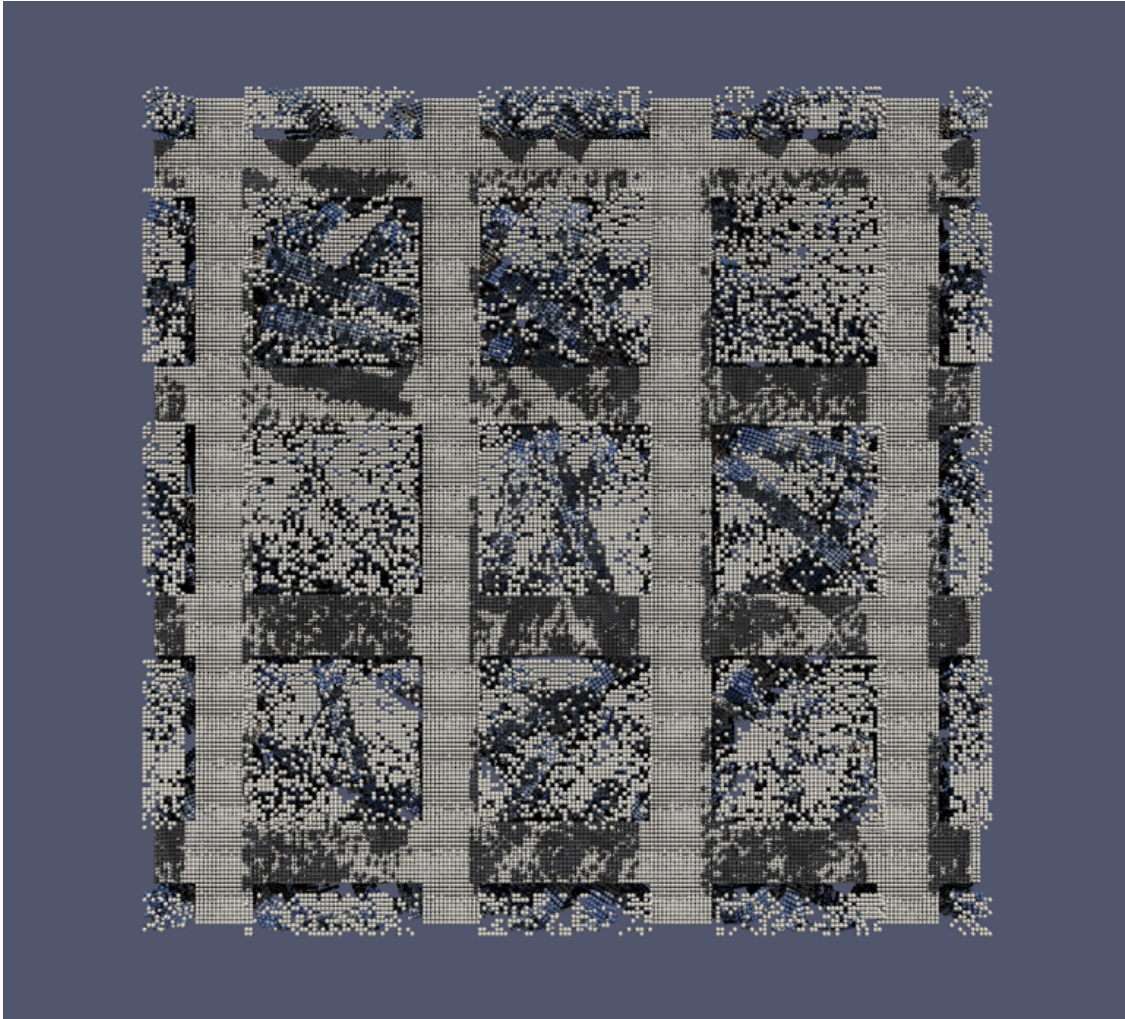
Figure 6.14. Fines Bottom View. This figure demonstrates how the system might be used to simulate fine retention through sieving.
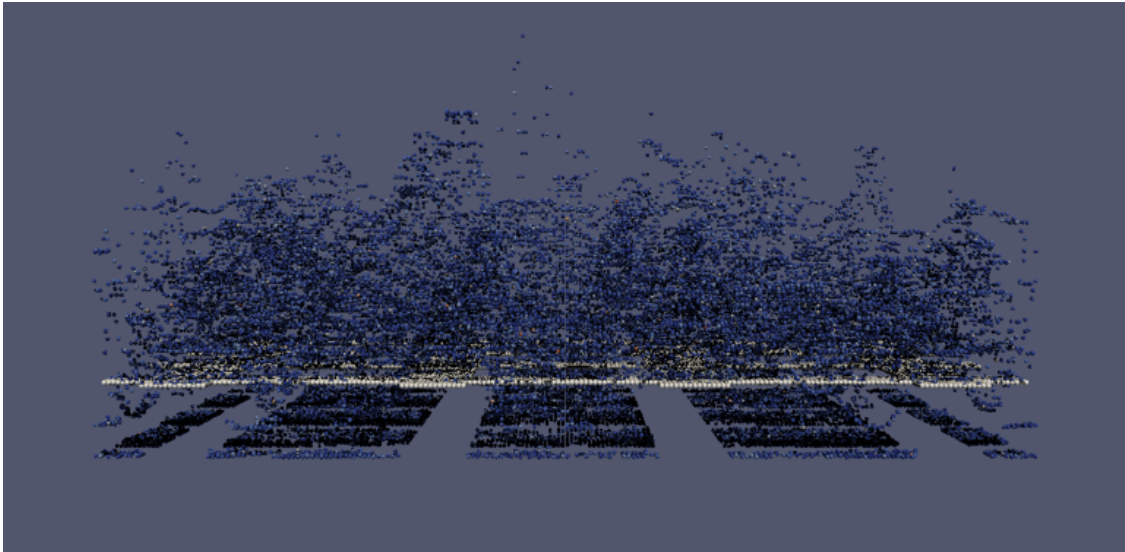
Figure 6.15. Fines With Fibers Removed. This figure shows the spatial distribution of fine particles retained by the structure.

CHAPTER 7
CONCLUSIONS AND FUTURE WORK

This work makes several notable advancements. The probabalistic representation of filtration and the multinomial model for the simultaneous placement of many fines described in chapter three have not previously been used to describe paper sheet formation. The technique adds realism to random particle placement simulations by representing the chaotic dynamics and realism to inputs by providing an efficient way to incorporate thousands of small particles into the structure simultaneously. The curvature minimization method for fiber placement is previously undescribed and enhances the realism of the PAKKA model with small additional computation. The additional realism yields good agreement with lab measured thicknesses suggesting additional property prediction is promising. Furthermore, the implementation described here achieves a balances of speed and realism heretofore unseen in the fiber packing literature.

Most generally, results show that a collection of simple rules can lead to large varieties of rich structures resembling those found in nature. This suggests complex models may be unnecessary to make useful predictions about the distribution of outcomes of chaotic systems if the right rules can be determined. Time spent developing and upgrading a model needs to be weighed against benefit relative to other activities like experimentation. Although more realism is desirable it may not appreciably enhance prediction. Addition of many capabilities allows for fine tuned differentiation between structures but unraveling many interconnected relationships inhibits timely practical prediction. Given some mild calibration capability, as long as the simulations yield distinct structures when their real world counterparts exhibit distinct properties it is not critical, but still desirable, for simulation to identically replicate experiment.

Possibly the primary constraint on realism is computation time. Many fluid and particle dynamics can be explained through first principles but this requires already

complicated partial differential equations of fluid flow to interact with dynamic complex boundary geometries of the particles. However such systems are generally intractable on relevant time or length scales. Fundamental to the efficiency of this model are the simplification of the problem into a probability measure of the final particle placement and minimization of the particles potential energy. Many simplifications made in the construction of the model fiber for the optimization problem are made to preserve the convexity of the cost function and solution space. However, the placement of a fiber of fixed length onto a random topography is inherently not convex. As the center of the fiber is moved relative to the random topography below, the cost function does not change but the constraint function changes in a non-linear fashion. Unfortunately, the issue of elongation, although minimized by the addition of a non-convex optimization step, still persists. The full effect it has on realism is unknown, but by construction, the volume of the fiber is conserved. So, elongation has the effect of decreasing the apparent thickness of a fiber, decreasing the the thickness as slope deviates from zero.

Even if the model can never provide an exact replication of the inspiring natural mechanics, it can still be calibrated to give useful results by tuning available parameters. Sheet thickness is easily observed, both experimentally, and through simulation, and is therefore a good starting point for model calibration. The simulated result space has good agreement with experimental space, suggesting the simulation could be easily calibrated for prediction. Notably, the adjustment of input parameters to the fibers can be adjusted to simulate the results of different processing steps. For example, the formation step might be simulated using stiffer fibers of equal height and width. Independently, the result of the combined formation and wet pressing steps can be obtained by increasing the width of the fiber, decreasing the height, so as to conserve fiber volume, and decreasing the stiffness of the fiber to represent additional force during pressing.

Rigorous calibration of model to experimental data is non-trivial and out of scope but should be considered a priority if the end modeling goal is practical property prediction.

Subtle differences in the natural density and flexibility distributions and their relationships need to be understood. While present simulation results have demonstrated good agreement with experimental observations and can explain a substantial amount of variation, more work is necessary to determine if single valued fiber properties provide good predictions or if the full distribution needs to be encoded. Although fiber length appears to have only a minor effect on thickness, its relationship to downstream properties like tensile strength means the full detail of the fiber dimension distribution should be described. Characterization of input distributions is incomplete at this time and model validation will require more carefully tuned experiments in the lab.

Currently, only the thickness of the structures is considered. While thickness is significant, enhancing other properties like stiffness, tensile or air permeability adds more value to the product. These properties are generally, computationally difficult to predict, however, one goal of this project is the generation of representative structures for use in future analysis. Given web structures generated using this simulation as a substrate, techniques like lattice Boltzmann simulation for coating studies or discrete element method for tensile strength and bending stiffness prediction can be used.

Furthermore, the richness of information stored within the structures has not been fully explored. While results can be summarized in terms of descriptive statistics or other easily computed quantities, they also contain a description of the fiber network and the pore network. From the list of points, the fiber, and pore connection networks can be determined. Developing techniques to process and quantify this information should enhance downstream property predictions. Understanding how these networks affect relevant physical properties and understanding how the networks might be tuned through mixing different particle and fiber types can lead to more optimized recipes.

We share several quantities of interest, relative bonded area, total curvature, a proxy for pore size estimates, total uncovered topography area. This is only a handful of possibly computable quantities. A superficial literature review of computational geometry and

55

image analysis yields many more interesting analysis designed for 3-d and bitmap data. Prediction of real world properties from simulated structures can likely be further enhanced by exploring the value of such derived quantities as predictors of hard to compute properties.

Finally, in addition to optimizing the application value of Maine's most abundant and sustainable natural resource, this project can have other impacts. Randomness and complex three-dimensional structures, both characteristics of paper, are common in many other natural phenomena. While paper is cheap and easy to make and test, other systems, like tissue growth, may not be. Techniques developed to deal with these challenges on a simple platform like paper can pave the way for more complex applications.

REFERENCES

[1] A.O. Ong'iro, V.I. Ugursal, A.M. Al Taweel, and D.K. Blamire. Simulation of combined cycle power plants using the aspen plus shell. *Heat Recovery Systems and CHP*, 15(2):105 – 113, 1995.

[2] M. Khoshnoodi and Y.S. Lim. Simulation of partial oxidation of natural gas to synthesis gas using aspen plus. *Fuel Processing Technology*, 50(2):275 – 289, 1997.

[3] Anders Sand, Martti Toivakka, and Tuomo Hjelt. Influence of colloidal interactions on pigment coating layer structure formation. *Journal of Colloid and Interface Science*, 332(2):394 – 401, 2009.

[4] Sergiy Lavrykov, Stefan Lindström, K Singh, and Bandaru Ramarao. 3d network simulations of paper structure. *Nordic Pulp and Paper Research Journal*, 27:256–263, 01 2012.

[5] J. D. Bauer and Frank R. Graziani. Statistical closure and the logistic map. *Phys. Rev. E*, 49:192–198, Jan 1994.

[6] Thomas Byholm, Martti Toivakka, and Jan Westerholm. Effective packing of 3-dimensional voxel-based arbitrarily shaped particles. *Powder Technology*, 196(2):139 – 146, 2009.

[7] W.W. Sampson. The structural characterisation of fibre networks in papermaking processes - a review. *In proc. The Science of Papermaking, (C.F. Baker, ed.), Trans. 11th Fund. Res. Symp.*, pages 1205–1288, 2001.

[8] K. J. Niskanen and M. J. Alava. Planar random networks with flexible fibers. *Phys. Rev. Lett.*, 73:3475–3478, Dec 1994.

[9] N Nilsen, M Zabihian, and K Niskanen. Kcl-pakka: a tool for simulating paper properties. *Tappi Journal*, 81:163–166, 05 1998.

[10] K Niskanen, N Nilsen, E Hellen, and M Alava. Kcl-pakka: A simulation tool for paper properties. *The Fundamentals of Papermaking Materials*, pages 1273–1292, 09 1997.

[11] Eduardo L. T. Conceição, Joana M. R. Curto, Rogério M. S. Simões, and António A. T. G. Portugal. Coding a simulation model of the 3d structure of paper. *Computational Modeling of Objects Represented in Images Lecture Notes in Computer Science*, page 299–310, 2010.

[12] Athmane Bakhta, Sébastien Leclaire, David Vidal, François Bertrand, and Mohamed Cheriet. Multiscale simulation of ink seepage into paper: A mesoscopic variational model. *Computer Physics Communications*, 239:1 – 13, 2019.

[13] B. Aurela and J. A. Ketoja. Diffusion of volatile compounds in fibre networks: experiments and modelling by random walk simulation. *Food Additives & Contaminants*, 19(sup1):56–62, 2002. PMID: 11962715.

[14] S van der Walt, S C Colbert, and G Varoquaux. The numpy array: A structure for efficient numerical computation. *Computing in Science Engineering*, 13(2):22–30, March 2011.

[15] T E Oliphant. Python for scientific computing. *Computing in Science Engineering*, 9(3):10–20, May 2007.

[16] Eric Jones, Travis Oliphant, Pearu Peterson, et al. SciPy: Open source scientific tools for Python, 2001–.

[17] J D Hunter. Matplotlib: A 2d graphics environment. *Computing in Science Engineering*, 9(3):90–95, May 2007.

[18] Utkarsh Ayachit, Berk Geveci, and Lisa Avila. *The ParaView guide updated for ParaView version 4.3*. Kitware, 2015.

[19] Richard H. Byrd, Peihuang Lu, Jorge Nocedal, and Ciyou Zhu. A limited memory algorithm for bound constrained optimization. *SIAM Journal on Scientific Computing*, 16(5):1190–19, 09 1995.

[20] D. Kraft. A software package for sequential quadratic programming. 88-28, 1988.

BIOGRAPHY OF THE AUTHOR

Tyler was born June 2nd 1989 in Lancaster New Hampshire to parents Dana and Lynn Seekins. He was raised in Glenburn Maine and attended Bangor High School, graduating in 2007. Tyler received his B.S. in Chemical Engineering from the University of Maine in 2011. After graduation he joined the DuPont Field Engineering Program, through which he spent two years in Richmond Virginia, receiving a Six Sigma Black Belt certification from the DuPont Protection Technologies business, and two years at the Experimental Station in Wilmington Delaware in the Industrial Bioscience Precommercial Process Development Group developing pilot and commercial scale process flowsheets and production schedules. Tyler returned to the University of Maine Chemical and Biomedical Engineering Department as Master's candidate in 2017. Upon graduation, He will be continuing his studies with advisor Dr. Douglas Bousfield in pursuit of a Doctorate of Philosophy in Chemical Engineering where he will focus on the use of machine learning to enhance simulation, prediction, and optimization in chemical processes. In his free time, Tyler enjoys staying active, especially skiing and snowboarding, painting, and programming.

Tyler R. Seekins is a candidate for the Master of Science degree in Chemical Engineering from the University of Maine in May 2019.